Title
Characterization of biogenic amine production by human gut associated bacteria

Author
Williams, Brianna Burden

Publication Date
2014

Peer reviewed|Thesis/dissertation

Characterization of biogenic amine production by human gut associated bacteria

by

Brianna Burden Williams

DISSERTATION

Submitted in partial satisfaction of the requirements for the degree of

DOCTOR OF PHILOSOPHY

in

Chemistry and Chemical Biology

in the

GRADUATE DIVISION

of the

UNIVERSITY OF CALIFORNIA, SAN FRANCISCO

ACKNOWLEDGMENTS

I need to start by thanking Dr. Richard Weiss at UCLA for accepting me into the MS^2 program and helping me get into a lab quickly as well as the Stanford Summer Research Program the summer after my first year in college. Dr. Weiss has been an amazing source of encouragement and support through all of my years in research and I would not be where I am today if it were not for him.

Second, I want to thank Dr. Bill Weis at Stanford University for accepting me into his lab despite my extreme lack of knowledge and experience. During my stay in his lab I discovered my passion for research through our troubleshooting discussion on how to get a protein interaction assay to work. I truly admire Bill and all of his success and thank him for a great experience that changed my career plan from physician to scientist.

I am also indebted to the mentorship of Dr. Brian Shoichet, for offering assistance at a very sensitive time during my graduate school tenure. My career will forever be more successful because of his advice.

I would also like to thank all of my former research mentors: Dr. Arthur Arnold, Dr. James Bowie, Dr. Harold Monbouquette, Dr. Linda van Aelst, and Dr. Warner C. Greene.

Specifically for the work outlined in this thesis, I would like to thank my mentor Dr. Michael A. Fischbach for providing all of the reasons why I shouldn't join his lab but ultimately accepting me anyway. He has been an excellent mentor, who despite chaotic situations, was always "calm about it", and spent several of our meetings google

searching. He ultimately provided a productive environment for me to complete my thesis.

I would also like to thank:

Ryan Ritterson for welcoming me into the Kortemme/Fischbach/Krogan neighborhood and sharing reagents and information with me when the Fischbach lab was still in its infancy, as well as doing all the manly things like pulling the 9.1 rotor out of the centrifuge and opening our gas tanks when there were no dudes in the lab.

Isa Munoz-Arias and Brian Webster for their support and friendship during my time in the Greene lab as well as during my time in the Fischbach lab.

Mao Taketani for spending an exhaustive amount of time trying to knockout CLOSPO_02083 during her rotation and then answering all of my questions while I tried to do it.

Mike Zimmermann for setting up the lab at UCSF and discovering the production of tryptamine by *Clostridium sporogenes*.

Sonnenburg lab: Purna, Jessica, Stephen for answering my questions, performing mouse experiments, and collecting mouse feces for me to analyze.

Fischbach lab members: Mohamed Donia, Jan Claesen, Yug Varma, and Tiffany Scharschmidt for never complaining that I talk too much.

I would also like to thank my thesis committee, Dr. Brian K. Shoichet, Dr. Alexander Johnson, and Dr. Charles Craik, for their encouragement and scientific guidance throughout the course of my graduate work.

For funding I would like to thank the NIGMS/IMSD training grant and the NSF Graduate Research Fellowship Program.

I would like to thank my parents and sister for supporting and encouraging me throughout the duration of my PhD despite their poor understanding of what I actually do. They can finally stop asking me when I am going to graduate.

Finally, I would like to thank my amazing husband, Dr. Segun Williams, who refused to add my name to his thesis and forced me to write my own.

Portions of chapters 1, 2, 3, and 5 of this thesis contain material previously published:

Williams, B.B., Van Benschoten, A.H., Cimermancic, P., Donia, M.S., Zimmermann, M., Ishihara, A., Fraser, J.S., Fischbach, M.A., *Discovery and characterization of two tryptamine-producing decarboxylases from the gut microbiota.* Cell Host and Microbe, in press.

Abstract

While the composition of the gut microbiota varies markedly among humans, the functional ramifications of these differences have only begun to be explored. In the course of characterizing the reductive metabolism of aromatic amino acids by a common gut Firmicute, *Clostridium sporogenes*, we made the unanticipated discovery that this bacterium decarboxylates tryptophan to form the β-arylamine neurotransmitter tryptamine, an enzymatic activity that is exceedingly rare among bacteria. Using a combination of genetics and biochemistry, we identify and characterize the PLP-dependent decarboxylase responsible for this activity, CLOSPO_02083, which had been misannotated as a tyrosine decarboxylase. To explore whether tryptophan decarboxylation is more widely distributed among the microbiota than previously known, we carried out a phylogeny-informed screen of ~15 putative bacterial decarboxylases. This screen revealed another novel tryptophan decarboxylase, RUMGNA_01526, which is phylogenetically distinct from CLOSPO_02083. Crystal structures of RUMGNA_01526 in its native form and bound to the inhibitor (*S*)-α-fluoromethyltryptophan, the first structures of a bacterial PLP-dependent decarboxylase, reveal the determinants of selectivity for the larger substrate Trp, including a flexible catalytic loop that controls access to the substrate-binding pocket. A computational analysis of whole-genome shotgun sequencing data from the Human Microbiome Project demonstrates that at least 10% of the human population harbors one of these two tryptophan decarboxylases in their gut community. By revealing a novel biochemical activity that is present in the gut communities of some but not all individuals, our results open a new line of investigation into the production and function of β-arylamines by the human microbiota.

Table of Contents

List of Tables

List of Figures

Chapter 1—Introduction

The human microbiome

The human body contains nearly 10 times the number of bacteria than human cells, a number approaching 10^{13}-10^{14}. These microorganisms inhabit various body sites and collectively contain more than 150 times the number of genes as the human genome, nearly 3.3 million (1). The majority of these bacteria reside in the gastrointestinal tract, which can contain up to 1000 different species in some individuals. The gut microbiome is largely composed of two bacterial phenotypes, *Bacteroidetes* and *Firmicutes*. Variations in community composition have been associated with several diseases including obesity, diabetes, and the intestinal bowel diseases (2-5). Molecules produced by the microbiota are essential for proper function of several physiological processes including harvesting energy from food sources, immune system development, and cardiovascular health.

One class of molecules produced by gut microorganisms is the short-chain fatty acids (SCFA). Colonic bacteria metabolize complex carbohydrates that are unable to be absorbed in the small intestine into acetate, propionate, and butyrate (6). The host epithelial cells are able to absorb these molecules via the G-protein coupled receptors GPR41 and GPR120 (7). Sensing of these molecules can increase secretion of leptin and GLP-1, peptide hormones that can regulate energy expenditure increase insulin release, respectively (8).

Additionally, the study of germ-free mice has highlighted the enormous contribution the gut microbe community has on the development of the immune system.

In addition to extreme morphological differences, germ-free mice have a compromised intestinal barrier, decreased plasma cells and IgA, and smaller mesenteric lymph nodes than conventionally raised mice (9-12). However, colonization with only one bacterial strain, *Bacteriodes fragilis*, is able to correct immune defects such as T cell deficiencies and lymphoid organogenesis through the release of polysaccharide A (PSA) (13). PSA binds to TLR2 and elicits appropriate cytokine production, restoring the balance of T-helper cells in the gut (14).

Most recently, an association between gut bacteria and cardiovascular function has been made. For years a correlation has existed between high consumption of red meat and cardiovascular disease. Recently, Koeth et al showed that a molecule found most abundantly in red meat, carnitine, is metabolized by gut bacteria into trimethylamine, which is then converted by the liver into trimethylamine oxide (TMAO)(15). The authors show that increased levels of TMAO increase the amount and severity of atherosclerosis.

Although the presence of microbes in the gut has long been known, the molecules they produce that influence host physiology are just recently being characterized. A small handful of molecules have been identified and characterized to have very significant effects on host physiology. However, one aspect of host health that could be influenced by the gut microbiota that remains without a molecular connection is the nervous system. Communication between gut organisms and the brain could occur via enteric nervous system.

Enteric Nervous System

The autonomic nervous system is divided into three components: sympathetic, parasympathetic, and enteric. The predominant role of the enteric nervous system (ENS) is neuronal modulation of gastrointestinal function (16). The significance of neuronal control of gut function is evidenced by the fact that both the ENS and the spinal cord contain approximately the same number of neurons. These neurons innervate the layers of intestinal epithelial cells and are able to control a variety of functions such as motility, microcirculation, peristaltic reflex, and immune and inflammatory processes (17). The primary connection between the gut and the brain is through the vagus nerve.

In 2004, Sudo et al demonstrated for the first time that commensal microbes affect the neural network responsible for the stress response (18). The authors were able to show that the presence of bacteria altered neurochemistry. By comparing germ-free and specified pathogen free (SPF) mice, they observed increased levels of both ACTH and corticosterone and decreased levels of BDNF expression levels in the cortex and hippocampus after a restraint stress test. By colonizing germ-free mice with a strain of bacteria known to colonize mice within the first days of life (*Bifidobacterium infantis*), these effects were reversed, indicating a role for microbes in the early development of the stress response. Since microbes are not known to colonize the brain, we speculate that bacteria in the gut are producing molecules that directly or indirectly alter brain chemistry.

Most recently, a convincing study by Bravo et al showed that the probiotic strain *Lactobacillus rhamnosus* could reduce anxiety in mice (19). After treatment with *L. rhamnosus*, conventionally raised mice have reduced stress-induced levels of

corticosterone. Additionally, they also show reduced expression of $GABA_{B1b}$ mRNA, similar to the effect of $GABA_B$ receptor antagonist antidepressants. Moreover, the authors do not observe these effects when the primary neuronal connection between the gut and the brain is severed, suggesting that signals from the gut are communicated to the brain directly through the vagus nerve.

The microbiota have also been implicated to play a role in the pathology of neurodevelopmental disorders, specifically autism spectrum disorder (ASD). ASD is a neurological disorder whereby affected individuals suffer from various physical and behavioral abnormalities. Clinical studies have correlated the severity of ASD with GI distress, including altered GI motility and increased intestinal permeability. Hsiao and colleagues used the maternal immune activation mouse model (which displays symptoms of ASD), to implicate a role for *Bacteroides fragilis* in the development of autism (20). They show that symptom severity is correlated with the *B. fragilis* metabolite 4-ethylphenylsulfate, establishing a molecular connection between the microbe and the host.

Together, these studies convincingly show that gut microbes are influencing the nervous system. However, at this time no molecular mechanism has been elucidated as to how these effects are achieved, nor have the participating genes been identified. Our interest lies in understanding what microbe-produced molecules are capable of generating neuronal responses. Due to their simplistic biosynthesis as well as interesting physiology, a sensible place to start our search is by looking at biogenic amines.

Biogenic amines

Biogenic amines are a class of molecules that contain several neurotransmitters including serotonin, tryptamine, tyramine, and phenethylamine. These molecules are produced by a single decarboxylation reaction from aromatic amino acids, which are readily available to gut organisms. Several of the decarboxylated amino acids comprise the class of molecules known as the trace amines, because they have only been detected at very low levels. However, a unique receptor, the Trace Amine Associated Receptor (TAAR), has been weakly characterized to respond to these molecules, suggesting that they do play a uniquely important role (21).

Anaerobic bacteria that colonize the gut are capable of metabolizing amino acids. The characterization of tyramine production by bacteria is particularly well studied as it occurs in several organisms involved in food preparation, especially the *Lactobacillus* species (22). However, most of the studies rely on strain production of tyramine without identifying the gene involved. Relatively recently Marcobol et al identified the gene in *Enterococcus faecalis* responsible for tyramine production and discovered it was also able to decarboxylate phenylalanine (23). These results led us to believe that we would be successful in finding microbes known to inhabit the human gut capable of generating neurotransmitter-like biogenic amines.

Chapter 2—Identifying bacterial amino acid decarboxylases

Introduction

Serendipitously while studying the metabolism of tryptophan by *Clostridium sporogenes*, we discovered that this bacterium was able to decarboxylate tryptophan into tryptamine. While several strains of bacteria have been shown to metabolize amino acids into amines, the excretion of tryptamine is exceedingly rare and the genes responsible have never been identified (24). Because of this, we were very interested in identifying the genes responsible. With this information, we could probe the human microbiome for additional bacterial contributors to the pool of biologically active tryptamine. At this time, the role of tryptamine has not been extensively characterized in the gut; however demonstrating that bacteria in the gut can produce observable quantities would open the door for probing the physiological, and neurological, role of microbial produced tryptamine.

Results and Discussion

Production of tryptamine by C. sporogenes

We started our journey seeking to identify molecules produced by a gut Firmicute that had antibiotic activity against a gut Bacteroidete. To do this, we cultured *C. sporogenes* and performed an organic extraction of the supernatant. Bio-assay guided fractionation led us to identify indole acetic acid as an antibiotic against the common gut strain *Bacteroides fragilis*. While the activity itself is interesting, we wanted to know the

genes responsible for production so that we could then look for other gut strains that contain the genetic material to produce the same molecule. We reasoned that tryptophan might be the starting material since both contain an indole ring. Our predictions proved to be correct, such that when we fed *C. sporogenes* tryptophan, indole acetic acid was produced. However, two additional molecules were also produced (Figure 2.1). Using LCMS and NMR, we confirmed that they were indole lactic acid and tryptamine. Although Wikoff et al confirmed an increase in plasma levels of indole acetic acid after germ-free mice were colonized by *C. sporogenes,* our studies into the antibiotic activity of indole acetic acid, as well as indole lactic acid, came to a stop once we realized that the molecules inhibited the growth of *C. sporogenes* itself (25).

Figure 2. 1

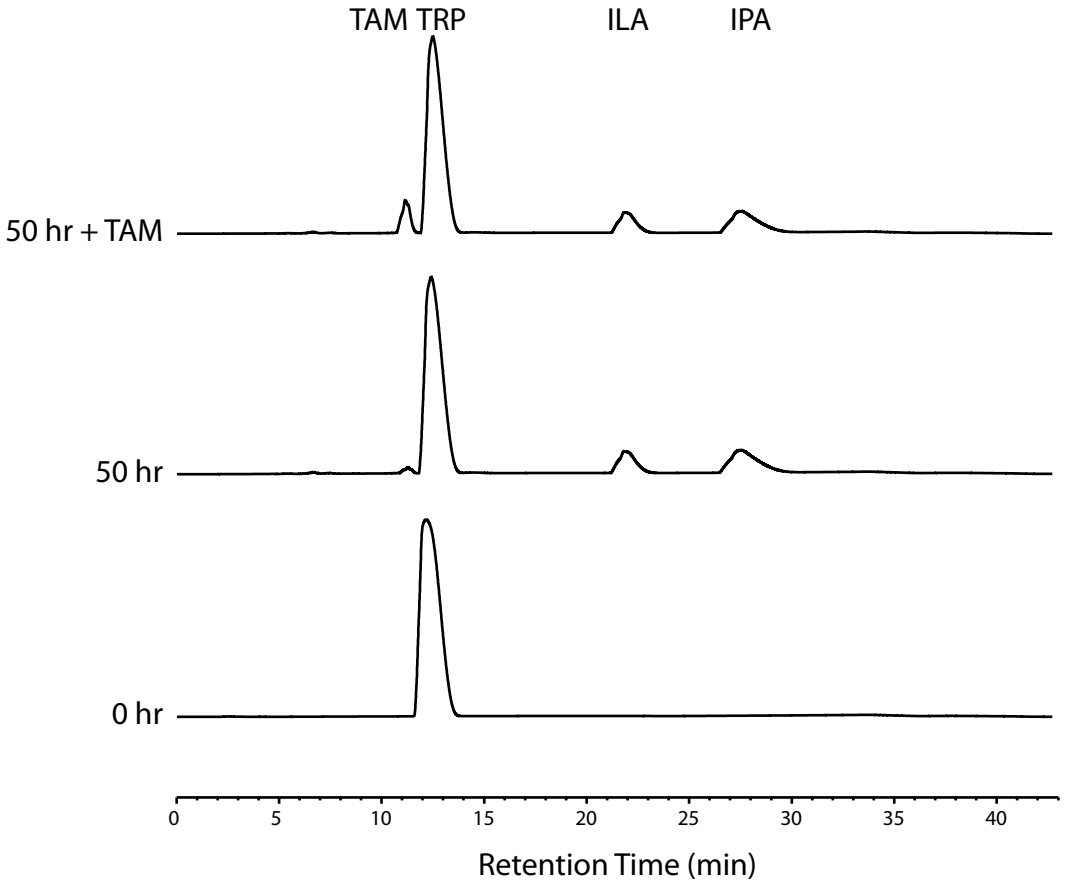

Figure 2.1 Production of tryptamine by C. sporogenes. Upon reaching confluency, C. sporogenes was transferred to minimal media containing 1 mg/mL tryptophan. After 50 hours of culture, three new molecules appear in the supernatant. To confirm the peak at ~11 min was tryptamine, a small amount of tryptamine was spiked into the supernatant and reanalyzed by HPLC.

However, the production of tryptamine was especially interesting given the significant structural similarity to serotonin, a potent neurotransmitter. Additionally, the presence of tryptamine in the culture fluid of *C. sporogenes* indicated that tryptamine was not only being produced but also exported from the cytoplasm to the extracellular space.

Identification of the tryptophan decarboxylase in C. sporogenes

We next set out to identify the enzyme responsible for tryptophan decarboxylation in *C. sporogenes* ATCC 15579. The two enzyme classes most commonly associated with amino acid decarboxylation are the pyridoxal 5'-phosphate (PLP)-dependent decarboxylases, in which the catalytic cycle begins with the covalent linkage of the substrate a-amine to PLP as a Schiff base, and the pyruvoyl-dependent decarboxylases, in which a covalently bound pyruvoyl cofactor arises from an autocatalytic posttranslational modification (26-28). A computational search of the *C. sporogenes* ATCC 15579 genome sequence revealed three putative PLP-dependent decarboxylases, but no putative pyruvoyl-dependent enzymes.

None of the three genes were annotated as tryptophan decarboxylases; CLOSPO_02083 was predicted to be a tyrosine decarboxylase, while CLOSPO_03076 and CLOSPO_00504 were predicted to be glutamate decarboxylases. We began by characterizing CLOSPO_02083, hypothesizing that its annotation might be correct and tryptophan decarboxylation was a secondary activity, or incorrect but close, since tyrosine and tryptophan are both aromatic amino acids. *E. coli* BL21 (DE3) harboring CLOSPO_02083 in the pET-28a expression vector were cultivated in rich medium and

grown to stationary phase. The cells were transferred into minimal medium containing tryptophan, and decarboxylation was monitored by analyzing cell-free culture fluid by analytical HPLC. After 24 hours, we saw complete conversion of tryptophan into tryptamine by CLOSPO_02083 (Figure 2.2)

Figure 2. 2

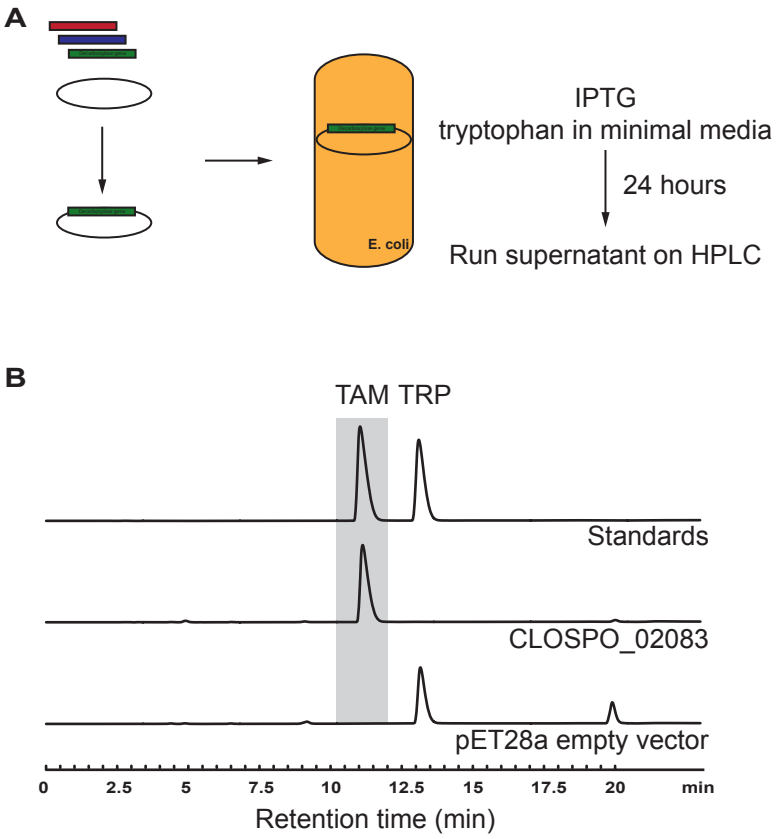

Figure 2.2 CLOSPO_02083 decarboxylates tryptophan (A) Schematic of experimental design to rapidly test several candidate decarboxylase genes in *E. coli*. (B) *E. coli* BL21 (DE3) harboring CLOSPO_02083 fully convert tryptophan into tryptamine within 24 hours.

Several other gut-associated *Clostridium spp.* harbor a homolog of CLOSPO_02083, but this enzyme does not appear to be present in other gut Firmicutes. We next asked whether there exist additional unrelated tryptophan decarboxylases among the human microbiota. A text search in Entrez Index using the query "tryptophan decarboxylase" yields protein hits exclusively from plant and fungal genomes, but the fact that CLOSPO_02083 was misannotated as a tyrosine decarboxylase led us to hypothesize that there might be other mis- or unannotated decarboxylases encoded by the microbiota that are tryptophan-selective.

A phylogeny-informed screen for additional tryptophan decarboxylases

To help us select a small panel of candidate decarboxylases from the microbiota, we performed a phylogenetic analysis of bacterial decarboxylases in which protein sequences were grouped into clades in which members are predicted to share a similar (if not identical) substrate selectivity. We then selected 15 sequences in a manner that maximized our ability to search the functional space of microbiome decarboxylases: at least one sequence from each of the largest clades and three additional sequences from smaller clades (Figure 2.3). We obtained and cultivated each of the host organisms to isolate genomic DNA. The candidate decarboxylases were amplified by PCR, subcloned into the pET-28a expression vector, and heterologously overexpressed in *E. coli* BL21 as N-terminal His_6 fusion proteins.

Figure 2. 3

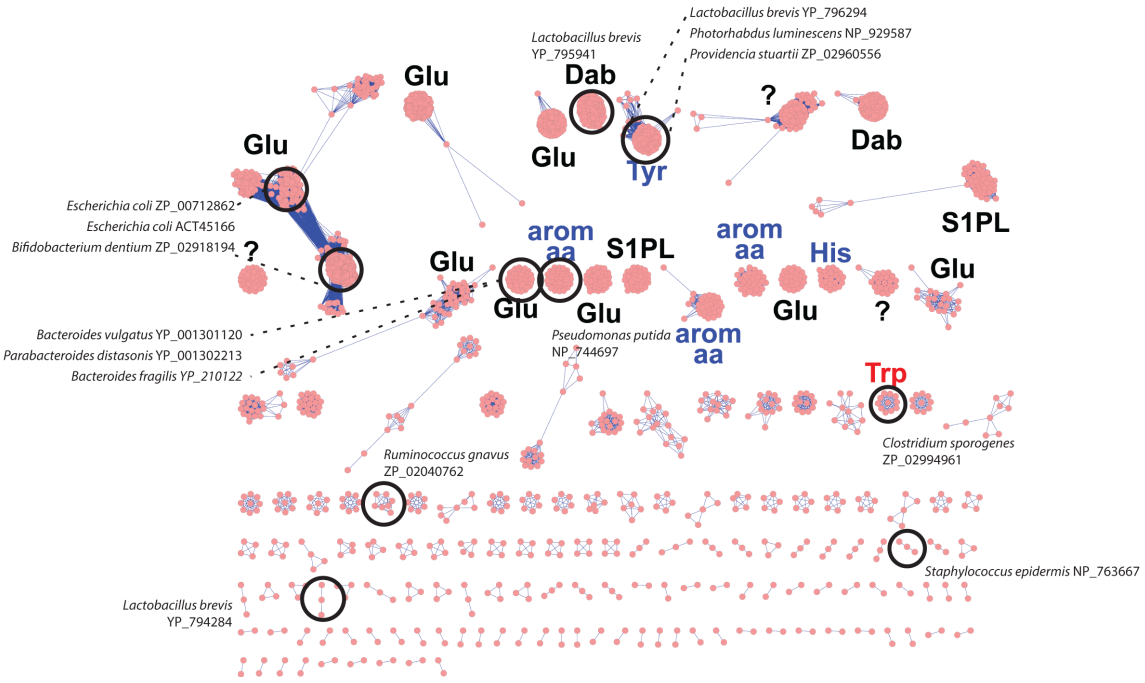

Figure 2.3 Cytoscape profiling results Sequences containing the consensus sequence for PLP-dependent decarboxylases in the database were clustered based on similarity. Enzyme substrates for each cluster were predicted based on annotations, and a representative subset of genes were selected for further analysis.

Since our aim was to discover new tryptophan decarboxylases rather than to obtain kinetic parameters for each enzyme in our screening panel, we developed and employed a whole-cell assay to rapidly assess the substrate selectivity of our candidate decarboxylases. *E. coli* BL21 (DE3) harboring candidate decarboxylases in pET-28a expression vectors were cultivated in rich medium and grown to stationary phase (Figure 2.2). The cells were transferred into minimal medium containing an aromatic amino acid substrate (tryptophan, tyrosine, phenylalanine, or histidine), and decarboxylation was monitored by analyzing cell-free culture fluid by analytical HPLC. This assay takes advantage of the fact that β-arylamines, the products of decarboxylase activity in the *E. coli* cytoplasm, could easily be detected in the extracellular fluid of *E. coli* cultures we screened and are not produced by wild-type *E. coli*.

An important limitation of the assay is that it is qualitative; in a manner that is likely due to differences in the level of active enzyme expressed, a more robust activity in the cell-based assay did not always translate into an enzyme with more efficient kinetic parameters. Moreover, we find that the assay detects low-level activities, which may indicate that activity is possible under specific yet-to-be-determined conditions and that the amino acid in question is not the preferred enzyme substrate.

Nevertheless, our qualitative assay enabled us to rapidly screen 15 decarboxylases against four substrates, summarized in Figure 2.4 as percent decarboxylation.

Figure 2. 4

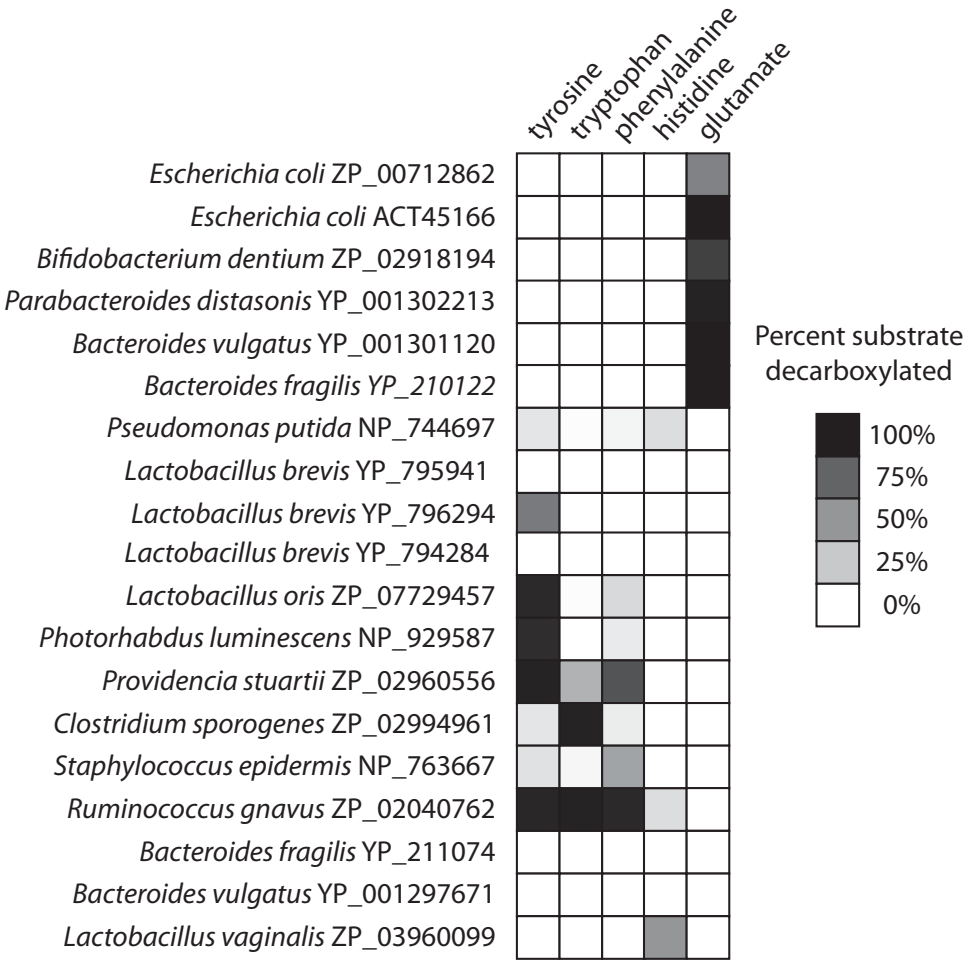

Figure 2.4 Summary of identified decarboxylase activity Percent substrate decarboxylated was determined by measuring the area under the curve for both the substrate (amino acid) and the product (amine). The percent substrate decarboxylated was calculated by taking the percent amine generated [amine/(amine+amino acid)] and illustrated on gray scale, setting 100% activity to 100% black.

Tyramine production

Bacterial production of tyramine has been well documented by the food industry. Indeed it is commonly found in fermented foods such as sausage and cheese. A disease called the "cheese syndrome" presents in patients taking monoamine oxidase inhibitors who eat tyramine-containing cheese which results in severe hypertension (29). Several genes demonstrated the ability to decarboxylate tyrosine, including *Pseudomonas putida* NP_744697*, Lactobacillus brevis* YP_796294*, Lactobacillus oris* ZP_07729457*, Photorhabdus luminescens* NP_929587*, Providencia stuartii* ZP_02960556*, Clostoridium sporogenes* ZP_02994961*, Staphylococcus epidermis* NP_73667*,* and *Ruminococcus gnavus* ZP_02040762.

Figure 2. 5

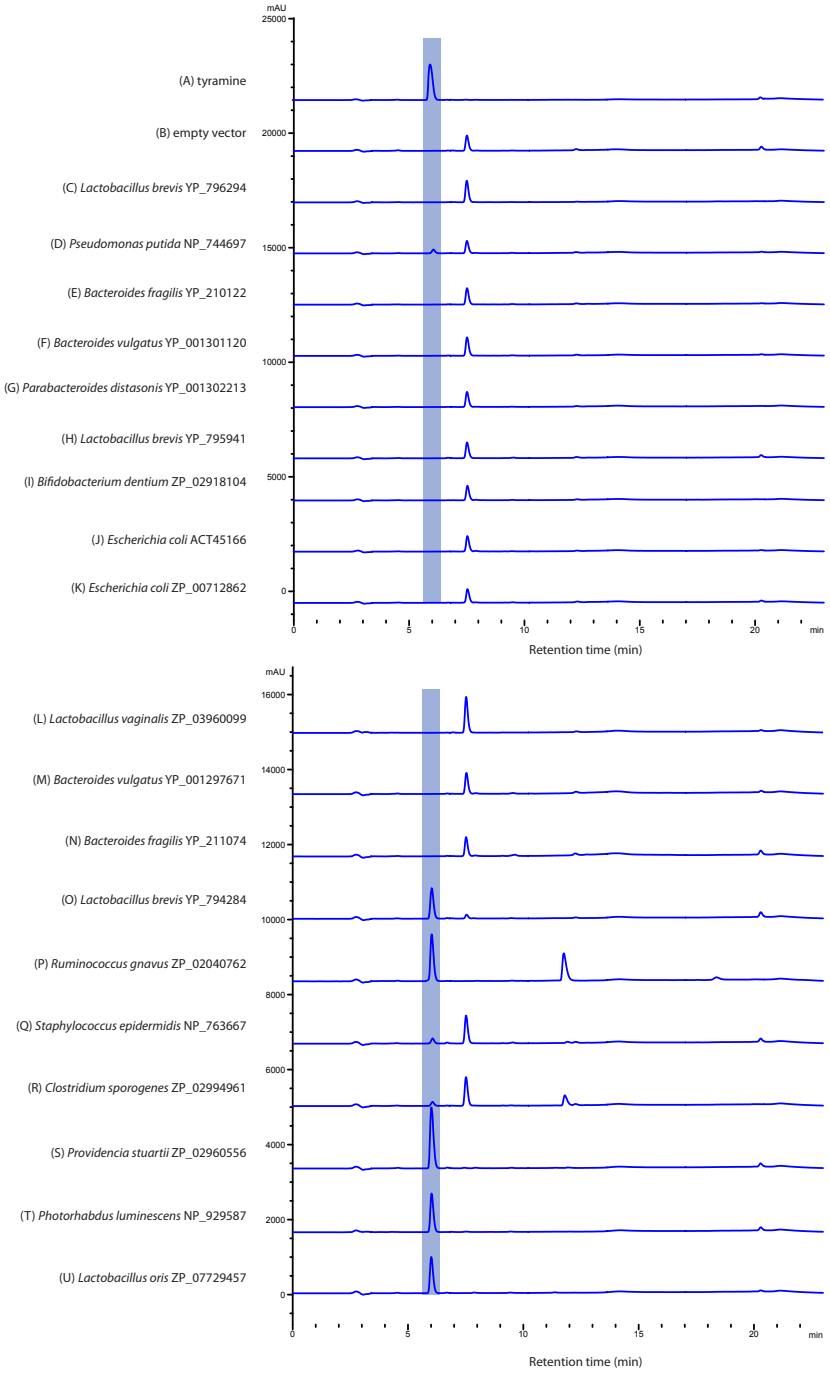

Figure 2.5 Tyrosine decarboxylase summary HPLC traces of clarified supernatant of *E. coli* BL21(DE3) harboring decarboxylase genes incubated in minimal media containing tyrosine. Tyramine highlighted in blue.

Phenethylamine production

All but one of the genes able to decarboxylate tyrosine could also decarboxylate phenylalanine. This was not surprising, as a similar gene has previously been described from *Enterococcus faecalis* (23). Only *Lactobacillus oris* ZP_07729457 was unable to produce phenethylamine.

Figure 2. 6

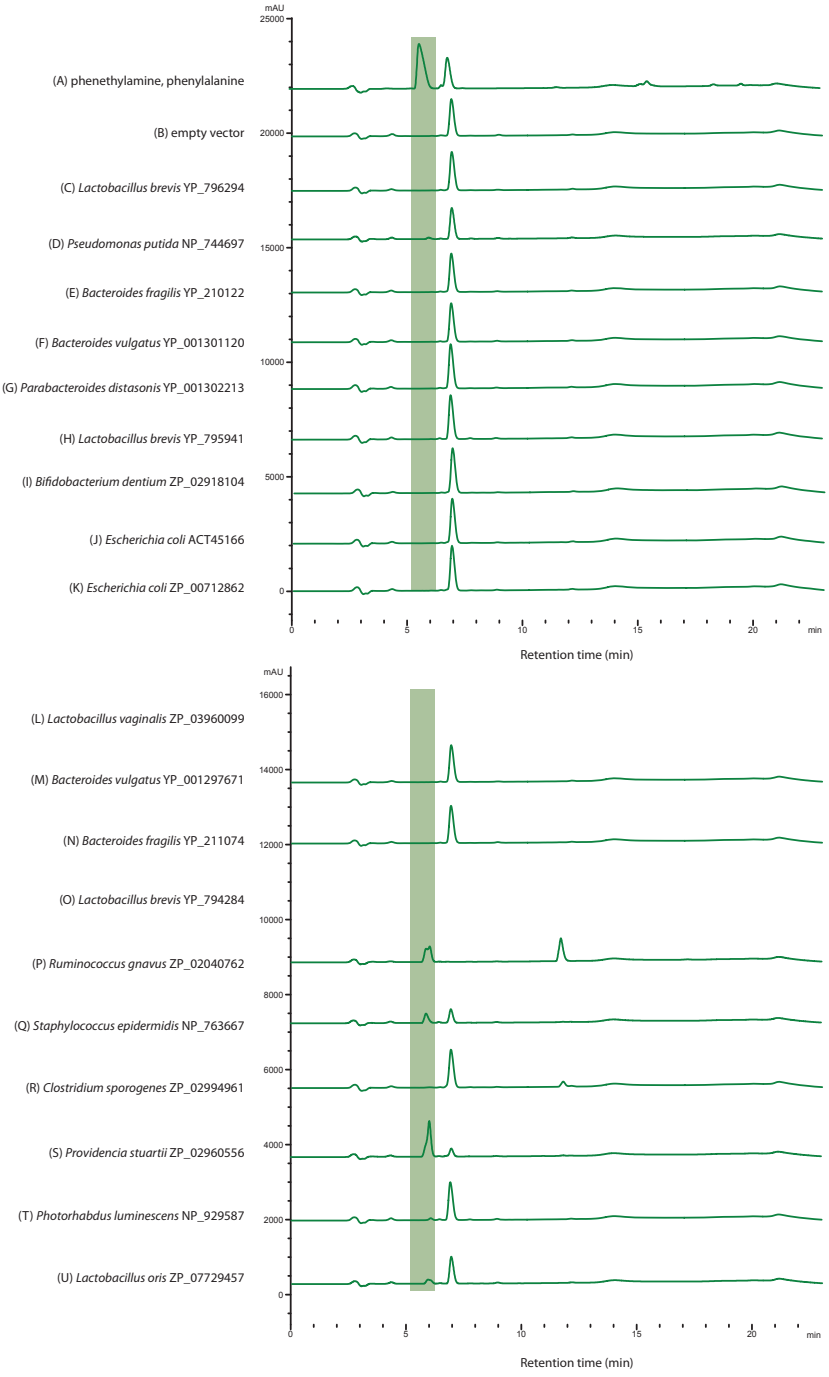

Figure 2.6 Phenylalanine decarboxylase summary HPLC traces of clarified supernatant of *E. coli* BL21(DE3) harboring decarboxylase genes incubated in minimal media containing phenylalanine. Phenethylamine highlighted in green.

Histamine production

Surprisingly, only two genes in our set were able to decarboxylate histidine: *Ruminococcus gnavus* ZP_02040762 and *Lactobacillus vaginalis* ZP_0396099. We had expected two genes from *Bacteroides*, YP_211074 and YP_0021297671 from *B. fragilis* and *B. vulgatus* respectively, to have activity since both strains have been shown in the literature to produce histamine. However, after multiple experimental strategies and attempts, no activity was shown.

Figure 2. 7

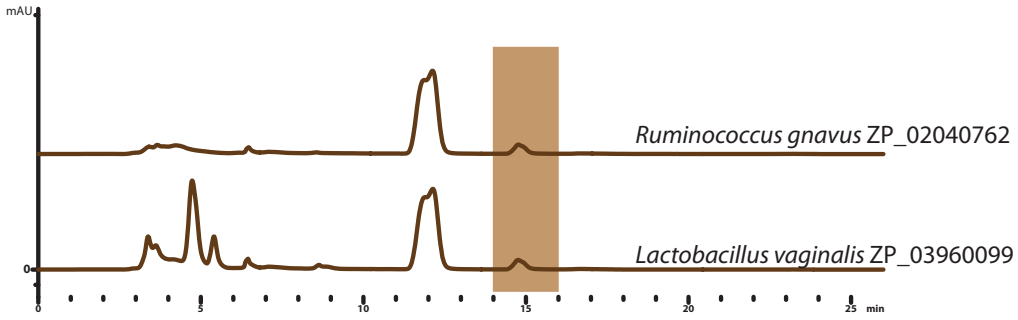

Figure 2.7 Histidine decarboxylase summary HPLC traces of clarified supernatant of *E. coli* BL21(DE3) harboring decarboxylase genes incubated in minimal media containing histidine. Histamine highlighted in brown.

Tryptamine production

Only three genes showed tryptophan decarboxylase activity: *Providencia stuartii* ZP_02960556*, Clostridium sporogenes* ZP_02994961*, and Ruminococcus gnavus* ZP_02040762 (Figure 2.8). The activity of *P. stuartii* against tryptophan is relatively weak and clusters most closely to *P. luminescens,* which has mainly tyrosine decarboxylase activity with low (<25%) phenylalanine activity and no tryptophan activity. This activity may carry over to other *Photorhabdus* strains that contain a similar gene (*P. rettgeri* DSM 1131*, P. asymbiotica asymbiotica* ATCC 43949*, P. rustigianii* DMS 4541*, P. alcalifaciens* DSM 30120).

The gene from *Clostridium sporogenes* is the only gene in the set that is selective for tryptophan. All other genes in the cluster belong to a strain of *Clostridium botulinum*, which is nearly identical to *C. sporogenes* except for the addition of the botulinum toxin genes. Most interestingly, we identified four substrates for *Ruminococcus gnavus* ZP_02040762: tryptophan, tyrosine, phenylalanine, and histidine. This strain of bacteria is found widely among the human gut microbiome, and could be a significant contributor of biogenic amines to the intestine. Notably, this enzyme was only very distantly related to CLOSPO_02083 (26% amino acid sequence identity). To confirm this result biochemically, we purified RUMGNA_01526 fusion protein by immobilized nickel affinity chromatography to >95% homogeneity (Figure 3.2).

Figure 2. 8

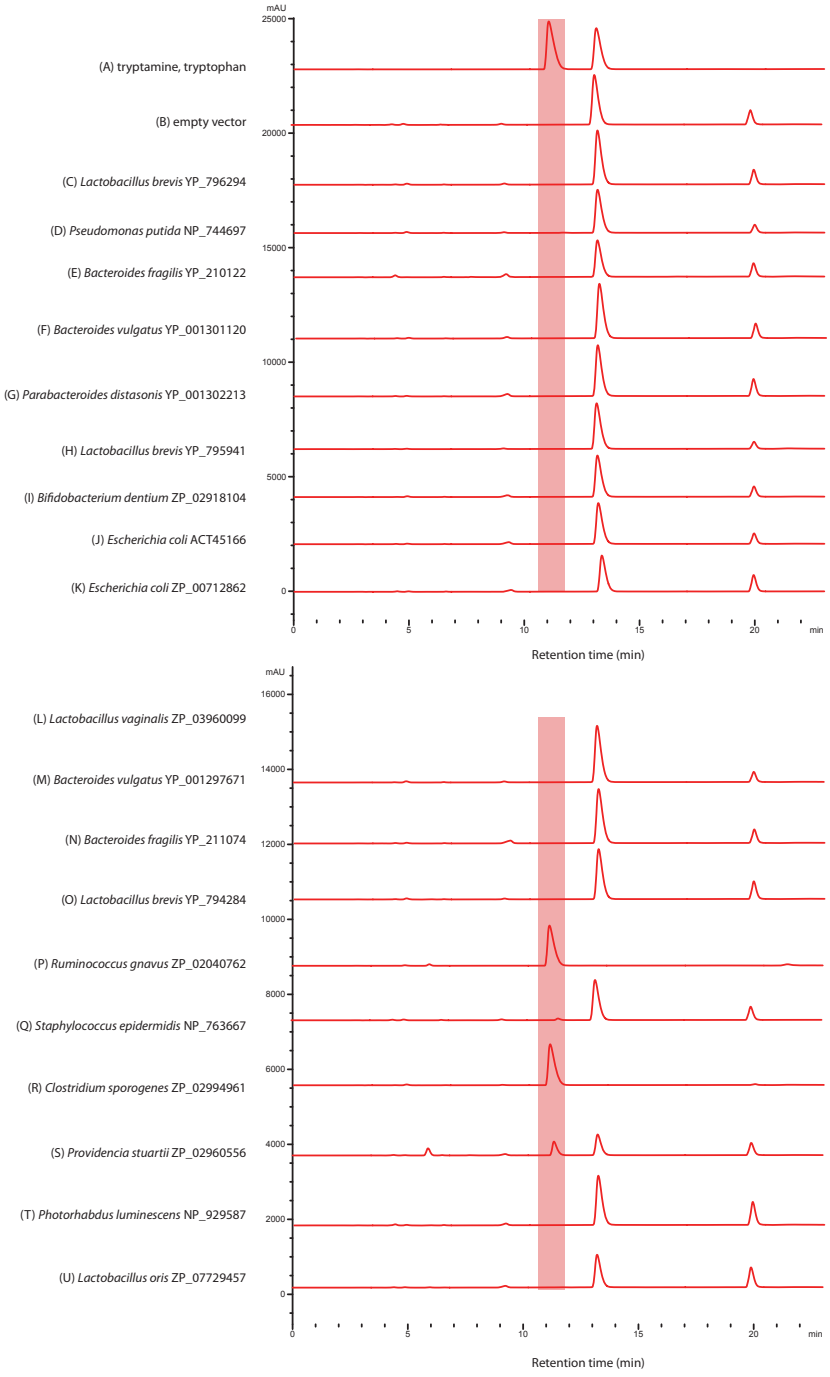

Figure 2.8 Tryptophan decarboxylase summary HPLC traces of clarified supernatant of *E. coli* BL21(DE3) harboring decarboxylase genes incubated in minimal media containing tryptophan. Tryptamine is highlighted in red.

GABA production

Testing for glutamate decarboxylase activity was more challenging than testing for aromatic amino acid decarboxylation. This was primarily due to the fact that the product of decarboxylation, GABA, was a substrate for several other enzymes and was readily degraded. It was also harder to analyze by HPLC as our detection method was not sensitive enough for a molecule without a chromophore. To overcome these challenges, we tested whole cell lysates in high substrate, low pH conditions. In endogenous conditions, bacterial decarboxylases are capable of regulating the pH of the environment through the release of carbon dioxide. The low pH used in the assay mimicked the endogenous conditions that these enzymes generally function in and allowed us the ability to test for activity.

We identified four glutamate decarboxylases: *Bifidobacterium dentium* ZP_02918194, *Parabacteroides distasonis* YP_001302213, *Bacteroides vulgatus* YP_001301120, and *Bacteroides fragilis* YP_210122 (Figure 2.9). We tested two *E. coli* genes, ZP_00712862 and ACT45166 as controls and they both demonstrated glutamate decarboxylase activity.

Figure 2. 9

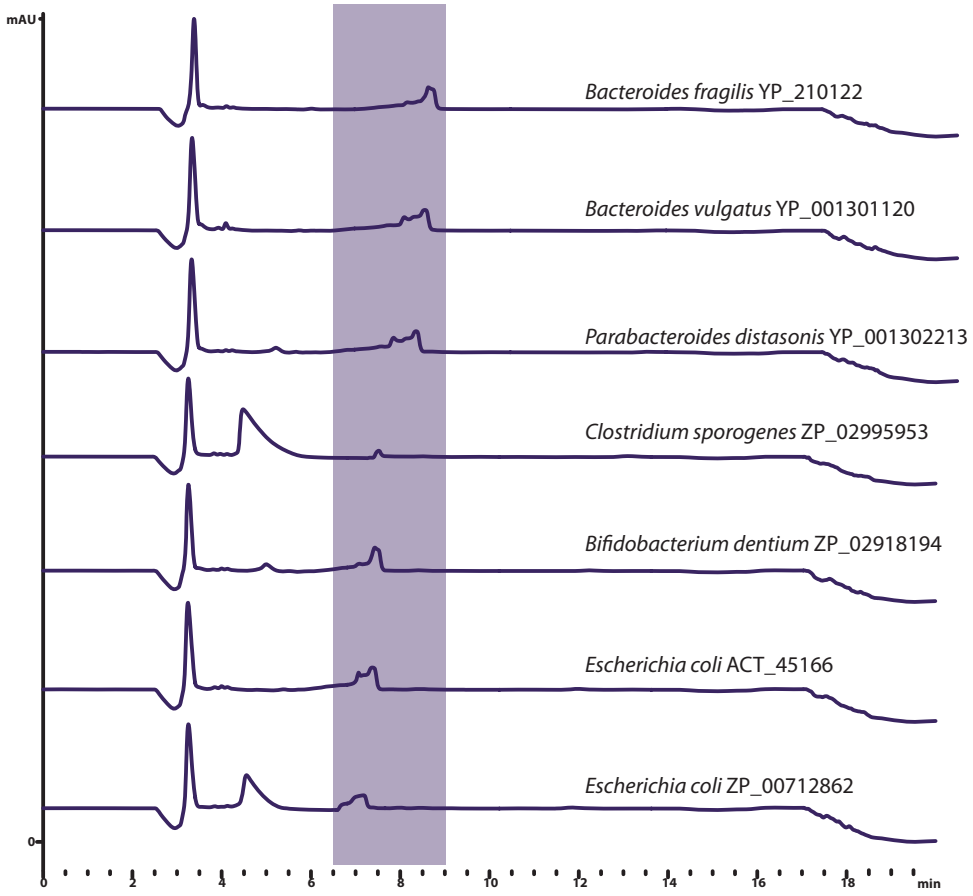

Figure 2.9 Glutamate decarboxylase summary HPLC traces of lysates of *E. coli* BL21(DE3) harboring decarboxylase genes incubated with glutamate at pH 3.0. GABA is highlighted in purple.

Strain decarboxylation

We showed above that *C. sporogenes* excretes the tryptamine generated by CLOSPO_02083 into the culture fluid. However, tryptamine produced in the cytoplasm could have a variety of alternative intracellular fates, including serving as a building block for the synthesis of a larger molecule. Having shown that RUMGNA_01526 is a tryptophan decarboxylase, we next asked whether *R. gnavus* excretes the tryptamine from RUMGNA_01526 into the extracellular space. We cultivated *R. gnavus* in rich medium until stationary phase, transferred the cell material into a defined minimal medium in the absence or presence of added tryptophan, and monitored the extracellular fluid by analytical HPLC. We observed that after 72 hours, the concentration of tryptamine reached ~1.7 mM (Figure 2.10), showing that *R. gnavus* excretes tryptamine in vitro and suggesting that this strain has the potential to excrete tryptamine in the ecological setting of the gut lumen. Additionally, production of tryptamine is not dependent on culture fluid pH.

We tested several other strains to confirm decarboxylase activity. However, only a subset of strains that contained genes that had activity in the *E. coli* assay were able to reproduce the decarboxylase activity. We saw that *Enterococcus faecalis, Lactobacillus brevis, Providencia stuartii,* and *Lactobacillus vaginalis* were able to recapitulate the activity seen in the *E. coli* assay. While these results confirm the activity of several decarboxylases, lack of activity does not exclude the possibility that the strains are able to produce the biogenic amine *in vivo*. There could be specific culture conditions that are necessary for gene expression and/or the enzymes could have more stringent substrate selectivity *in vivo*.

Figure 2. 10

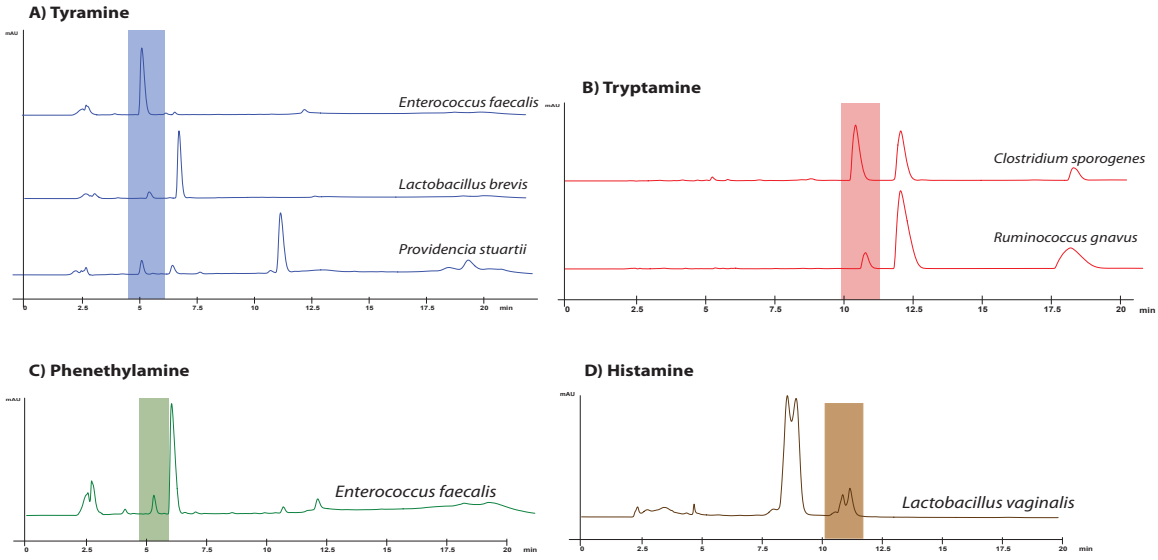

Figure 2.10 Strain decarboxylase summary Indicated strains of bacteria were grown in rich media to confluency and resuspended in minimal media containing the substrate of interest. After 24 hours, cell-free supernatant was analyzed by HPLC. (A) Production of tyramine (highlighted in blue) by *E. faecalis, L. brevis,* and *P. stuartii*. (B) Production of tryptamine (highlighted in red) by *C. sporogenes* and *R. gnavus*. (C) Production of phenethylamine (highlighted in green) by *E. faecalis*. (D) Production of histamine (highlighted in brown) by *L. vaginalis.*

Experimental Procedures

Cloning

Genomic DNA (gDNA) from each candidate organism was obtained by performing a standard Qiagen miniprep with the following substitution: 2% SDS was used instead of the P2 buffer and the sample was incubated at 55C for 25 minutes. PCR (Phusion, GC buffer, 1.5% DMSO) was performed using gDNA as the template as follows: 98C-5 minutes; 30 cycles of 98C-20s, 55C-30s, 72C-45s; 68C-5 minutes. PCR products were purified using a Qiagen MinElute kit and eluted in 15 μL EB. 2uL was used in a CPEC (circular polymerase extension cloning) reaction. pET28a was linearized with NdeI and XhoI, agarose gel purified using the Qiagen MinElute kit and eluted in 15 μL. 2 μL of a 1:4 dilution of the purified linearized vector was used in the CPEC reaction. The vector and insert were added to a PCR reaction and (20 μL) initially denatured at 98C for 30s, followed by six cycles of 98C for 10s, 55C for 30s and 72C for 3 minutes, with a final extension time at 72C for 5 minutes. 3 μL of the CPEC reaction was used to transform *E. coli* Tg1 cells. Positive colonies were used to inoculate 5 mL cultures and DNA was purified using a Qiagen MiniPrep kit. Following sequence confirmation, 1 μL of DNA was used to transform *E. coli* BL21 (DE3) cells for protein expression.

E. coli Expression Assay

5 mL cultures inoculated by glycerol stocks were grown overnight at 37C. In the morning, 500 μL of confluent culture was diluted into a fresh 5 mL of LB, and grown for 90 minutes at 37C. The culture was spun down for 10 minutes at 3750xg and resuspended in filtered M9 minimal media containing 1 mM IPTG and 5 mM of one of the following amino acids: tryptophan, phenylalanine, tyrosine or histidine. Cultures were grown at 37C overnight (~20 hours), except in the case of the histidine samples, which were grown for 72 hours. In the morning, 0.5 mL of culture was centrifuged and 100 μL of supernatant was injected onto the HPLC.

HPLC Methods

Samples containing tryptophan, phenylalanine, or tyrosine were analyzed by HPLC using a ThermoScientific Hypercarb column, (100 mm x 4.6 mm x 5um) at a flow rate of 1.0 mL/min, with a UV detector (220nm and 280nm). The mobile phase solvents included A (water), B (acetonitrile, ACN), C (isopropanol, ISP), and D (methanol, MeOH), all supplemented with 0.1% TFA (trifluoroacetic acid). The gradient elution had the following profile: 5-30.8% B, 5-30.8% C, and 2% D from 0 to 14 min; 30.8-49% ACN, 30.8-49% ISP, 2% MeOH from 14-17 min; and 49-5% B, 49-5% C, 2% D from 17-20 min; 5% B, 5% C, 2% D from 20-23 min. Standard elution times were as follows: tryptophan 13.0 min (280nm), tryptamine 11.0 min (280nm); phenylalanine 6.9 min (220nm), phenethylamine 5.6 min (220nm), tyrosine 6.8 min (220nm), tyramine 5.1 min (220nm). Retention time varied slightly over the years.

Samples containing histidine were analyzed by HPLC using a PolyLC Polyhydroxyethyl A column (200mm x 4.6mm x 5um), at a flow rate of 1.0 mL/min, UV detection at 205nm and ambient temperature. The mobile phases consisted of 2 solvents: A (95% ACN, 15mM Triethylamine phosphate pH 3) and B (5% ACN, 15mM Triethylamine phosphate pH 3). The gradient elution had the following profile: 35% B from 0 to 3 min; 35-82% B from 3-18 min; 82-100% B from 18-18.5 min; 100% B from 18.5-22 min; 100-35% B from 22-22.5 min, and 35% B from 22.5-26 min. Histidine had a retention time of 11.8 min and histamine at 14.9 min.

Glutamate decarboxylase assay

Proteins were expressed as described above. 24 hours after IPTG induction, 500 μL of culture was pelleted in a 1.5 mL centrifuge tube. Cells were resuspended in 500 μL 150 mM glutamate prepared in *E. coli* minimal media and adjusted to pH 3. Tubes were incubated at 37C for 35 minutes, centrifuged at 15k x g for 3 minutes, and analyzed by HPLC.

Supernatant from enzyme assays was analyzed by HPLC using a SiELC Primesep 100 column (150mm x 4.6mm x 5um) at a flow rate of 1.0 mL/min, UV detection at 205 nm at 20C. 100 μL was injected and elution was performed isocratically at 10% ACN followed by a column washing (100% ACN for 2.5 minutes) and re-equilibration (10% ACN for 3.5 minutes). The retention time of glutamate was approximately 4.6 min and GABA was 7.8 min.

Decarboxylation by parent strain

Cultures of originating strain were inoculated from a glycerol stock and grown in corresponding media for 24 hours. For anaerobic cultures, 15 mL of culture was transferred to a 15-mL conical tube, sealed, and pelleted by centrifugation. Supernatant was discarded and pellet was resuspended in 15 mL of filtered minimal media containing 5 mM of specified amino acid, and transferred back to a 14 mL culture tube. For aerobic cultures, 5 mL of culture was prepared and pelleted by centrifugation in 14 mL culture tube before resuspending in an equal volume of minimal media containing 5 mM amino acid. Please refer to appendix A for more specific growth conditions.

Chapter 3—Structure and kinetics of RUMGNA_01526

Introduction

Tryptophan decarboxylation is observed in several taxa including humans, flies, and plants. Despite the similarity to serotonin, tryptamine is not an intermediate in the synthesis of this abundant neurotransmitter in humans. The production of serotonin starts with hydroxylation of tryptophan, followed by decarboxylation, bypassing the tryptamine intermediate. The decarboxylase utilized in serotonin production (aromatic amino acid decarboxylase, AAADC) is capable of producing tryptamine; however very low levels are observed *in vivo* and a unique role for this amine has yet to be elucidated. On the other hand, in plants, tryptamine is required for several secondary metabolites (30, 31). Most notably, it is an important precursor for the plant hormone auxin, or indole acetic acid (32). It is also involved in alkaloid biosynthesis, an extensive family of molecules with a wide pharmacological activity profile (33).

Tryptophan decarboxylation in bacterial species is exceedingly rare and has only been characterized in a select few species. *Lactobacillus bulgaricus* was the first bacterial strain shown to directly excrete tryptamine (34). Two other strains produce tryptamine, but only as a building block for the biosynthesis of larger natural products: the nematode symbiont *Xenorhabdus nematophilis* and *Bacillus atrophaeus* (35, 36).

The proposed mechanism of tryptophan decarboxylation involves the formation of a Schiff base between pyridoxyal-5'-phosphate (PLP) and a lysine residue within the active site of the enzyme (Figure 3.1). Substrate binding releases PLP from the enzyme and decarboxylation results in a quinonoid intermediate. Protonation at the C_{α} position of

the substrate and a transaldimination reaction with the lysine residue releases the aldimine while regenerating the PLP-enzyme complex. PLP functions to stabilize anions generated at the C_{α} by delocalizing the negative charge in the pi system of the cofactor by resonance in the quinonoid intermediate (37-39).

Figure 3. 1

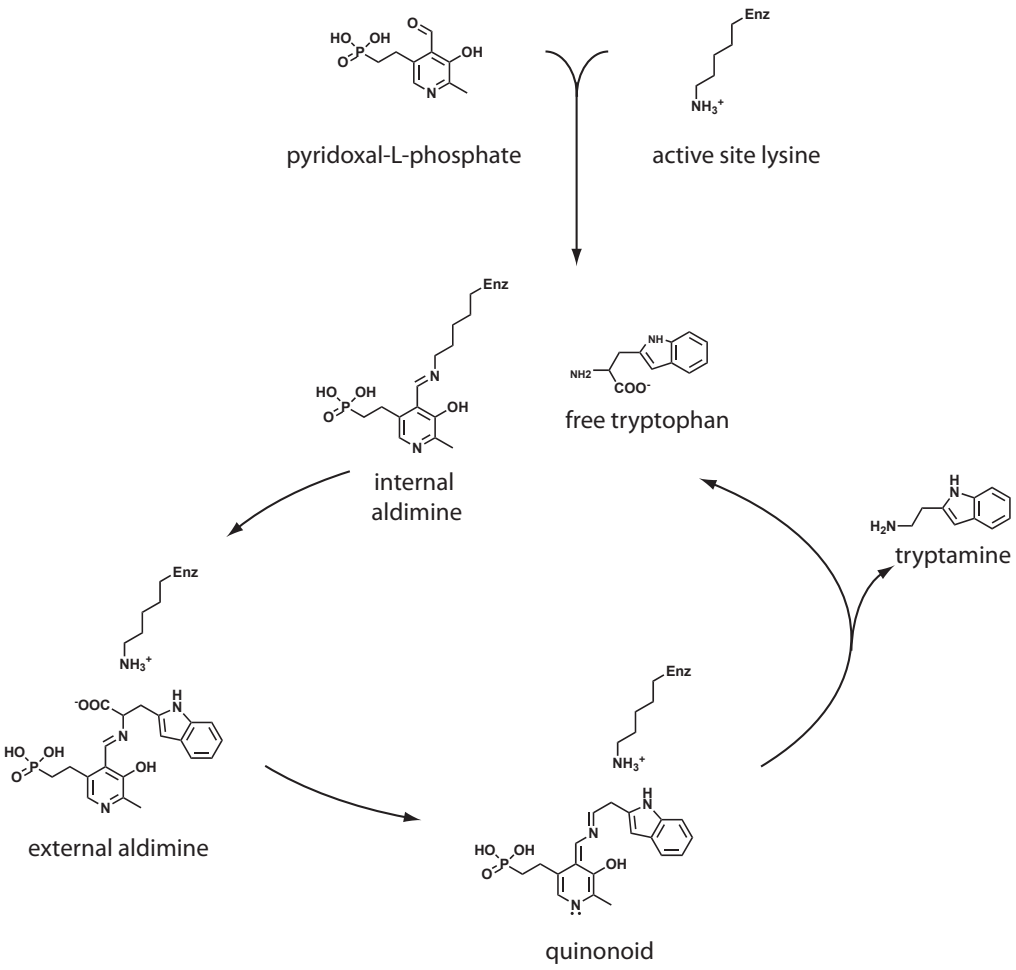

Figure 3.1 Mechanism of PLP dependent decarboxylation PLP covalently binds to the enzyme through an active site lysine residue, resulting in an internal aldimine. The enzyme is exchanged for the tryptophan substrate and the decarboxylated substrate is stabilized by a quinonoid intermediate. A transaldimination releases the tryptamine product and the PLP re-bonds to the active site lysine.

Several enzymes are dependent on PLP as a cofactor including: α,β,γ-synthases, aminotransferases, transaminating decarboxylases, serine hydroxymethyl transferases, and β-eliminases (26, 27). While the mechanisms between the enzymes vary, they all rely upon a quinonoid intermediate to delocalize the negative charge generated at C_{α}. Structurally, they fall into five fold types. The majority of enzymes are of Fold Type I, or the aspartate aminotransferase family, which is characterized by a homodimer where the active site resides in the dimer interface. Fold Type II is referred to as the tryptophan synthase family and functions as a dimer but the active site is contained within one monomer. Fold Types III (alanine racemase family) and IV (D-amino acid aminotransferase family) are structurally unique in that PLP binds in manner that is the mirror image of Fold Types I and II. Fold Type V is the glycogen phosphorylase family and utilizes an entirely different mechanism that relies on the phosphate group of PLP for catalysis (27).

We were first interested in confirming the substrate selectivity of both the *Ruminococcus gnavus* and *Clostridium sporogenes* enzymes by determining the kinetic parameters for several aromatic amino acid substrates. Additionally, we sought to determine their crystal structures to better understand the substrate selectivity and evolutionary origins of the enzymes.

Results and Discussion

Purification of RUMGNA_01526 and CLOSPO_02083

RUMGNA_01526 and CLOSPO_02083 were expressed in BL21 (DE3) cells at low temperature for 16-20 hours and purified by immobilized nickel affinity chromatography. Purified protein was visualized by SDS-PAGE and was estimated to be >95% pure (Figure 3.2). During preliminary kinetic and crystallography experiments, the enzymes appeared to lose activity over short periods of time (hours) and were therefore purified fresh for each experiment.

CLOSPO_02083 production was low when expressed under the same conditions as RUMGNA_01526. Fenalti et al added substrate (glutamate) and cofactor (PLP) to their media and purification solutions when purifying the glutamate decarboxylases (40). Adding 30 μM PLP to the LB media, lysis buffer, and elution buffer as well as10 mM tryptophan to the lysis buffer significantly enhanced production of CLOSPO_02083.

Figure 3. 2

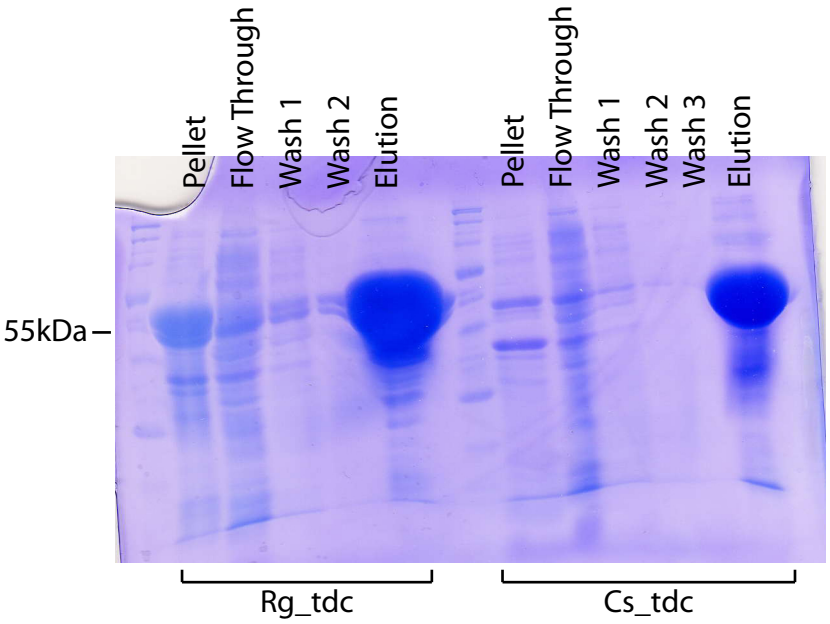

Figure 3.2 SDS-PAGE of purified RUMGNA_01526 and CLOSPO_02083 Nickel affinity chromatography was used to purify both RUMGNA_01526 and CLOSPO_02083. Samples from solubilized pellet, bead flow through, wash steps, and elution were loaded onto an SDS-PAGE gel and visualized by Coomassie staining.

Kinetic parameters of RUMGNA_01526 and CLOSPO_02083

The previous results in Chapter 2 show that CLOSPO_02083 is capable of decarboxylating tryptophan, but it does not rule out the possibility that one of the other aromatic amino acids is transformed more efficiently. To gain insight into the substrate selectivity of CLOSPO_02083, we measured the basic kinetic parameters for CLOSPO_02083-catalyzed decarboxylation of the aromatic amino acids tryptophan, tyrosine, and phenylalanine. To determine k_{cat} and K_m for CLOSPO_02083, the concentration of the amino acid substrate was varied under initial velocity conditions (Figures 3.3, 3.4). At 100 nM CLOSPO_02083, the K_m for tryptophan is 2.8 ± 0.0 mM and k_{cat} is 1199 min^{-1}, demonstrating that tryptophan is a robust substrate for decarboxylation. The activity of CLOSPO_02083 against phenylalanine was undetectable up to 90 mM substrate (Figures 3.3, 3.4). Although the limited solubility of tyrosine prevented us from obtaining kinetic parameters, at the highest concentration of tyrosine we tested, CLOSPO_02083 was 600-fold more efficient at decarboxylating tryptophan (Figure 3.3). Collectively, these results show that tryptophan is accepted more efficiently as a substrate than phenylalanine or tyrosine.

These results suggest that the database annotation of CLOSPO_02083 as a tyrosine decarboxylase is incorrect. The chemical distinction between tyrosine and tryptophan is mild, since they are both aromatic amino acids. However, the biological distinction between their decarboxylation products is sharp: tyramine stimulates a pressor response that results in an increase in blood pressure, whereas tryptamine induces the release of serotonin from enterochromaffin cells and stimulates GI motility (41, 42).

Thus, a modest difference in a decarboxylase's substrate selectivity can lead to entirely distinct biological outcomes, placing a premium on biochemically characterizing the substrate selectivity of amino acid decarboxylases expressed by gut commensals.

We measured the basic kinetic parameters for the decarboxylation of tryptophan, tyrosine, and phenylalanine by RUMGNA_01526. As shown in Figures 3.3 and 3.4, tryptophan is a robust substrate for decarboxylation, with a k_{cat} of 6048 min^{-1} and a K_m of 1.4 ± 0.1 mM at 20 nM enzyme. In spite of the robust activity of RUMGNA_01526 against tryptophan, tyrosine, and phenylalanine in the cell-based assay (Chapter 2), the catalytic efficiency of RUMGNA_01526 for tryptophan is >1000-fold higher than it is for phenylalanine (Fig. 2*D* and S7*B*), due to the combination of a higher k_{cat} (26-fold) and a lower K_m (50-fold). Although the limited solubility of tyrosine prevented us from obtaining kinetic parameters, at the highest concentration of tyrosine we tested, RUMGNA_01526 was 1500-fold more efficient at decarboxylating tryptophan. These data suggest that tryptophan is the native substrate of RUMGNA_01526.

Figure 3. 3

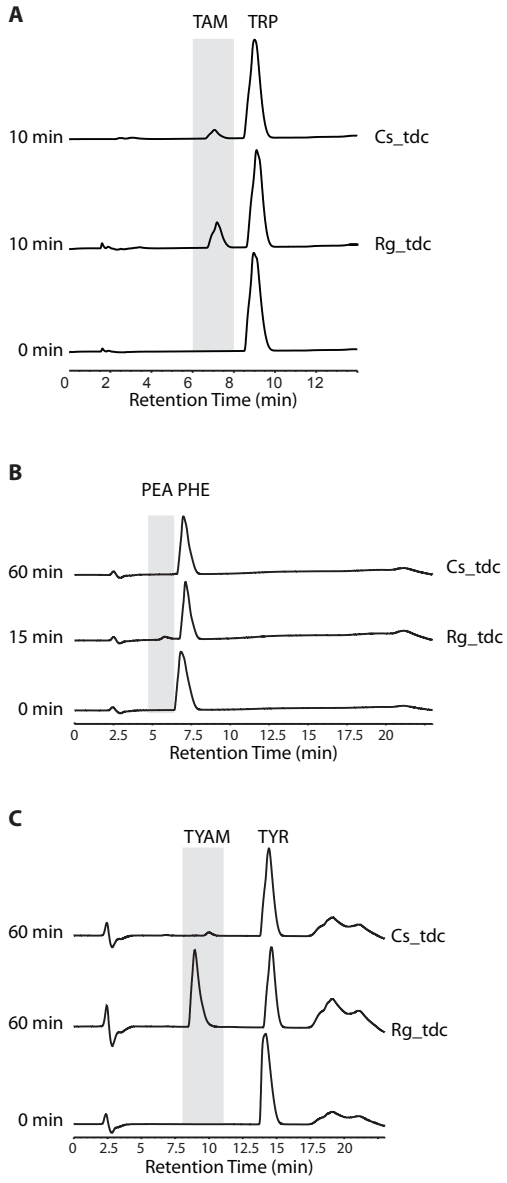

Figure 3.3 Biochemical activity of RUMGNA_01526 and CLOSPO_02083 Purified RUMGNA_01526 or CLOSPO_02083 was incubated with either (A) tryptophan (TRP), (B) phenylalanine (PHE), or (C) tyrosine (TYR) at 37C and quenched with 1 volume of methanol after the indicated time. 100 μL of clarified reaction mixture was analyzed by HPLC. The products tryptamine (TAM), phenethylamine (PEA) or tyramine (TYAM) are highlighted in gray.

Figure 3. 4

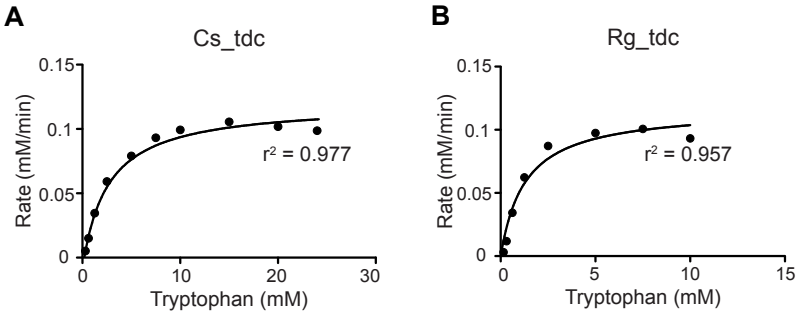

C

	Cs_tdc Tryptophan	Rg_tdc Tryptophan	Rg_tdc Phenylalanine
K_m (mM)	2.756 ± 0.027	1.386 ± 0.065	69.7 ± 6.6
v_{max} (mM/min)	0.119 ± 0.003	0.121 ± 0.004	0.116 ± 0.01
k_{cat} (min^{-1})	1199	6048	233.9
k_{cat}/K_m ($M^{-1}sec^{-1}$)	7.25×10^3	7.27×10^4	56

Figure 3.4 Kinetic analysis of RUMGNA_01526 and CLOSPO_02083 Rate versus substrate concentration curves for (A) CLOSPO_02083 or (B) RUMGNA_01526. (C) Summary of determined kinetic parameters.

Inhibition kinetics of RUMGNA_01526 and CLOSPO_02083

The close structural relationship between RUMGNA_01526 and glutamate decarboxylase raises the question of how the structural scaffold of RUMGNA_01526 accommodates the large, hydrophobic substrate tryptophan. Since the ideal approach to answering this question would involve determining the structure of RUMGNA_01526 bound to a tryptophan-mimicking inhibitor, we proceeded to determine whether a previously reported inhibitor of plant tryptophan decarboxylase, (*S*)-α-fluoromethyltryptophan ((*S*)-α-FMT, Fig. 3*A* **I**), was an inhibitor of RUMGNA_01526 (31).

Although mechanistic studies have not been performed to determine the mode of tryptophan decarboxylase inhibition by (*S*)-α-FMT, biochemical studies with a similar amino acid analog, (*S*)-α-fluoromethylhistidine ((*S*)-α-FMH), show that this inhibitor blocks histidine decarboxylase in a mechanism-dependent fashion that involves the formation of a covalent adduct between the inhibitor and PLP (43, 44).

We measured the production of tryptamine by HPLC in the presence of various concentrations of inhibitor over 30 minutes, and analyzed progress curves of the reaction to assess the kinetics of inhibition. Indeed, not only for RUMGNA_01526 but also for CLOSPO_02083, we observed linear progress curves in the presence of increasing concentrations of inhibitor, consistent with covalent inhibition (Figure 3.5). Despite having a comparable K_m for tryptophan, RUMGNA_01526 has a weaker affinity for (*S*)-α-FMT than CLOSPO_02083 (K_i of 178 mM vs. 0.2 mM). However, it is more rapidly inhibited (k_{inact} of 1.2 min^{-1} vs. 0.1 min^{-1}), suggesting that once the weak enzyme-inhibitor

complex forms, the relative orientation of PLP and the inhibitor is conducive to covalent bond formation (Figure 3.5).

Figure 3. 5

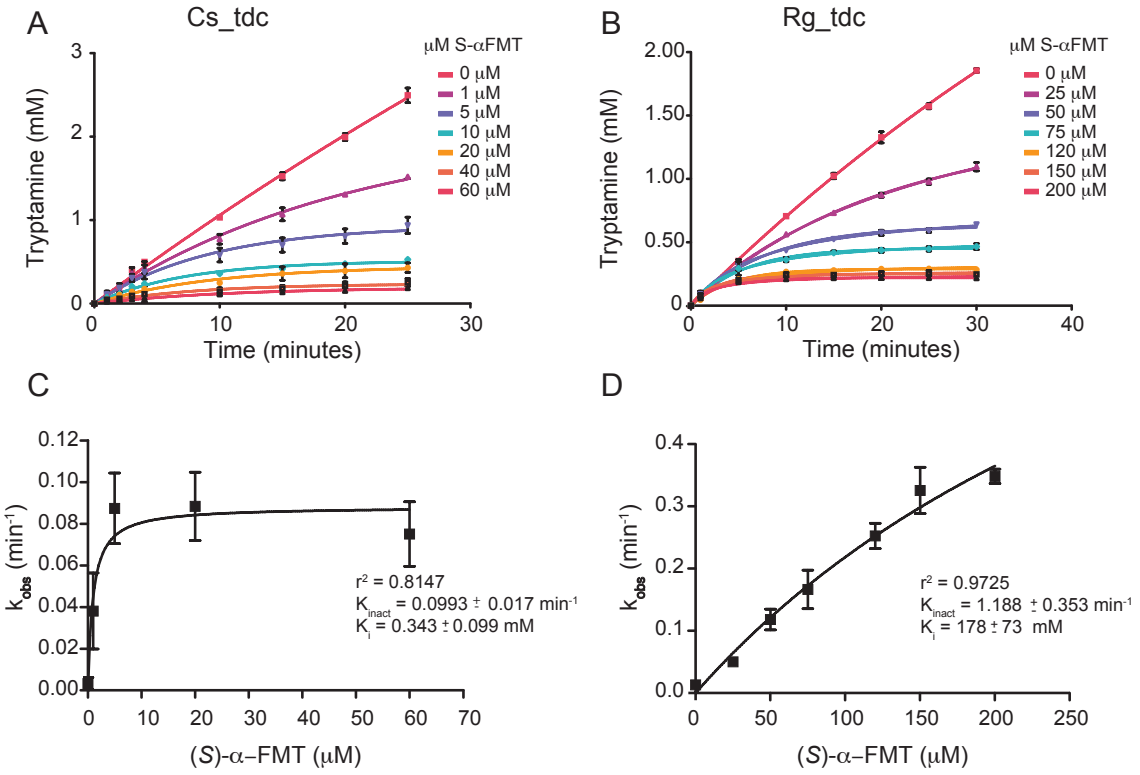

Figure 3.5 Inhibition kinetics of (*S*)-α-FMT against RUMGNA_01526 and CLOSPO_02083 Plot of product formed in the presence of varying concentrations of inhibitor versus time for (A) CLOSPO_02083 and (B) RUMGNA_01526. k_{obs} was determined from A,B and replotted versus substrate concentration for (C) CLOSPO_02083 and (D) RUMGNA_01526 to determine the inhibition kinetic parameters K_{inact} and K_i.

The inactivation of histidine decarboxylase by (*S*)-α-FMH is initiated by substrate decarboxylation followed by the elimination of fluoride ion. A transaldimination releases the enamine, which can react and inactivate the PLP cofactor. In order to elucidate the mechanism by which (*S*)-α-FMT inhibits RUMGNA_01526, as well as to understand how RUMGNA_01526 accommodates the large, hydrophobic substrate tryptophan, we sought to determine the X-ray crystal structure of the inhibitor-bound enzyme.

Crystallization of ligand free RUMGNA_01526

Initial screening of FPLC-purified RUMGNA_01526 against the JCSG CORE suites (Qiagen) produced hits in three conditions: (1) 1.4M sodium citrate, 0.1M sodium HEPES pH 7.5 (2) 0.2M potassium formate, 20% PEG 3350, and (3) 0.2M Lithium sulfate, 0.1M CAPS pH 10.5, 2M ammonium sulfate. Crystals from the 96-well screening plates were recovered and analyzed. Only condition (1) gave mild diffraction, but all three conditions were optimized. Unfortunately although several attempts at optimization were made, crystals never reproduced in these conditions. This was most likely due to the fact that the first trays were set up in a "quick and dirty" manner and several details were lost. After multiple rounds of troubleshooting with no success (including varying dialysis buffer composition, temperature, protein concentration, and pipetting conditions), we decided to repeat the screen.

The second round of JCSG CORE suite screening produced crystals in several conditions, but the most promising crystals were found in (4) 0.1M Bicine pH 8.5, 10% PEG 6000 (although no crystals were found in similar screening conditions A- 0.1M Bicine pH 8.5, 20% PEG 6000, B- 0.1M Bicine pH 8.5, 5% PEG 6000, and C- 0.1M

Bicine pH 8.5, 30% PEG 6000), (5) 0.1M Bicine pH 8.5, 25% PEG 3350, and (6) 0.2M di-sodium hydrogen phosphate, 20% PEG 3350. The crystals in these conditions formed very quickly (within hours); however they also dissolved over time. The only condition that produced stable crystals was condition (4), which convinced us to focus optimization around the bicine conditions.

We set up several optimization trays around conditions (4), (5), and (6), but consistently saw the best crystals in condition 0.1M Bicine pH 8.5, 25% PEG 3350 (exactly condition (5)). After selecting this condition, four cryoprotectants were tested: PEG 400, ethylene glycol, glycerol, and MPD. The final data set was obtained with crystals frozen in 10% glycerol.

Structure of RUMGNA_01526

We determined the crystal structure of RUMGNA_01526 at 2.8 Å, the first structure of a bacterial PLP-dependent decarboxylase (Figure 3.6A). The enzyme forms a dimer with 4565 $Å^2$ buried at the dimer interface. The active site is located at the dimer interface and therefore the enzyme is only functional in the dimeric state. The monomeric unit is comprised of three domains: an N-terminal domain containing three parallel α-helices that pack against the other monomer, a large domain comprised of a nine-stranded β-sheet surrounded by nine α-helices containing the PLP-binding site, and a smaller C-terminal domain comprised of a four-strand anti-parallel β-sheet surrounded by three α-helices. The active site reveals continuous electron density shows PLP covalently linked to K306 through a Schiff base (Figure 3.6C). The structure is nearly identical to the open

form of human glutamate decarboxylase (GAD65), with an overall α-carbon RMSD of 1.07 Å (40). Similar comparisons can be made to human aromatic amino acid decarboxylase and wild boar DOPA decarboxylase, with α-carbon RMSDs of 1.21 Å and 1.23 Å, respectively (45, 46). The agreement between these structures highlights the commonality of this enzymatic fold, even across multiple species.

Figure 3. 6

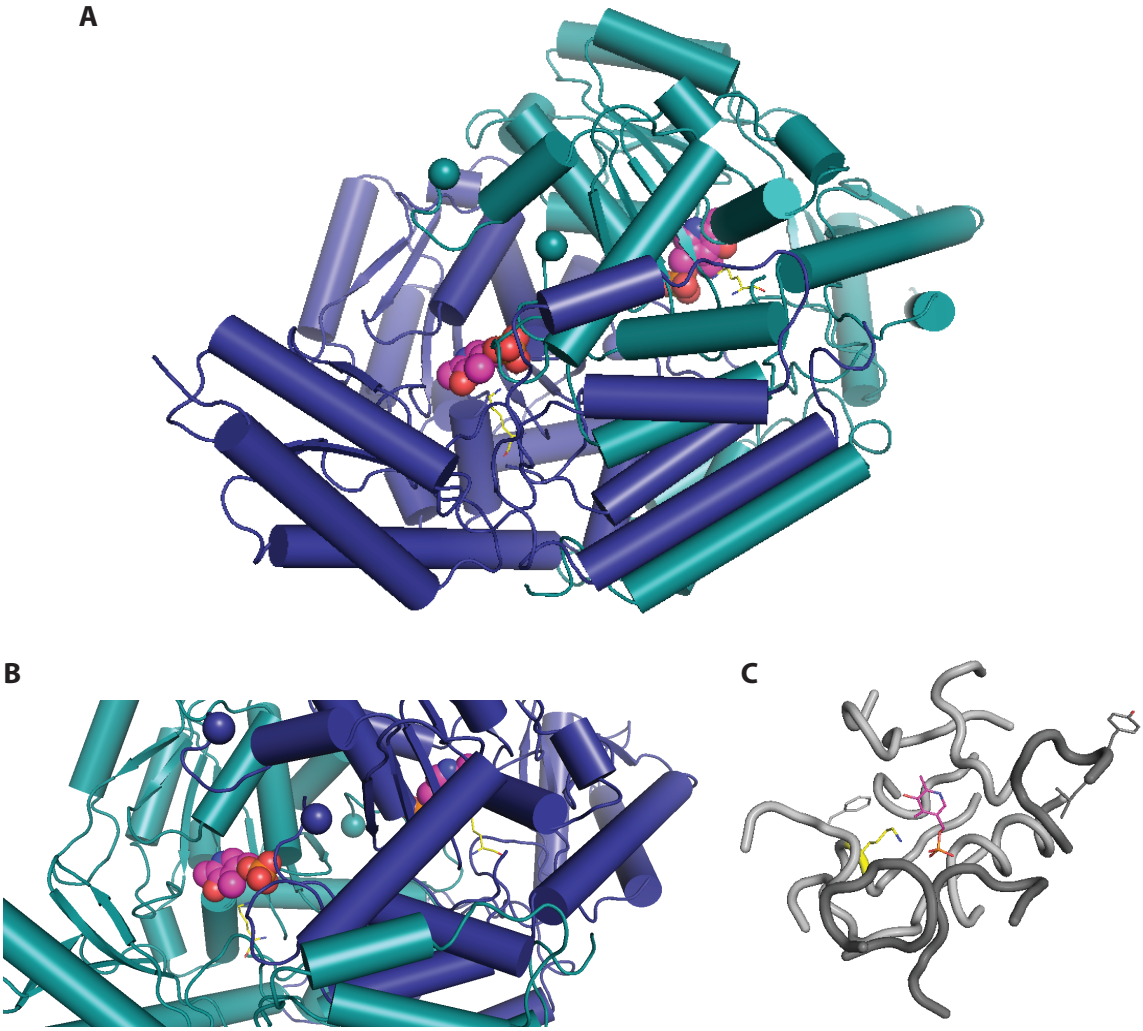

Figure 3.6 Structure of apo RUMGNA_01526 (A) Overall fold of RUMGNA_01526 reveals an obligate functional dimer. (B) The active site remains exposed in the absence of ligand (PLP shown as pink spheres) (C) Active site shows PLP bound to K306.

Crystallization of CLOSPO_02083

After relatively quick success of solving the structure of RUMGNA_01526, we attempted crystallization of CLOSPO_02083. We started by screening FPLC-purified protein against the JCSG CORE suites using the Mosquito to set up the trays and saw crystals in 6 conditions:

(1) 0.1M citric acid pH 4.0, 5% PEG 6000

(2) 0.1M citric acid pH 2.5, 20% PEG 6000

(3) 0.2M ammonium sulfate, 30% PEG 8000

(4) 0.2M magnesium chloride, 0.1M Tris-HCl pH 8.5, 30% PEG 4000

(5) 0.2M magnesium chloride, 0.1M Tris-HCl pH 8.5, 25% 1,2 propanediol, 10% glycerol

(6) 1.0M Lithium chloride, 0.1M citric acid, 30% PEG 6000

Unfortunately, several attempts at reproducing crystals were unsuccessful. Reasoning that the purification tag was interfering with crystallization, new constructs were made that would allow cleavage of the tag. This involved re-cloning into the same vector using different sites in the MCS that would reduce the space linker between the tag and the N-terminus of the protein.

Thrombin cleavage of the his-tag proved to be an important step in crystallization, as well as incubation with the inhibitor (*S*)-α-FMT. Screening against the JCSG CORE suites produced several hits after four days:

(1) 0.2M lithium sulfate, 0.1M CAPS pH 10.5, 2M ammonium sulfate

(2) 0.2M potassium thiocyanate, 20% PEG 3350

(3) 0.2M lithium phosphate, citrate pH 4.2, 10% PEG 3000

(4) 0.1M Tris pH 8.0, 40% MPD

(5) 0.2M ammonium dyhydrogen phosphate, 20% PEG 3350

(6) 35% dioxane

(7) 0.05M calcium acetate, 0.1M imidazole pH 8.0, 35% ethoxyethanol

(8) 0.1M sodium citrate pH 5.5, 35% ethoxyethanol

Optimization was performed on conditions (4), (5), (6), (7) and (8) and crystals were reproduced in all conditions except (5). However, none of the conditions produced crystals that were suitable for diffraction. The most promising crystals were from conditions (4) and (7). In order to improve crystal shape and size, the Hampton Research Additive Screen was used with these conditions. Three additives to condition (8) produced crystals with improved shape and size: (8A) 0.1M adenosine-5 triphosphate disodium salt, (8B) 40% v/v polypropylene glycol P400 and (8C) 40% v/v acetone. Further optimization around these additives produced crystals in conditions (8A) and (8B).

After multiple rounds of optimizing around crystallization solution, protein concentration, and inhibitor concentration, the most promising crystals were formed in 0.1M citrate pH 5.25, 35% ethoxyethanol, 0.1M ATP, 2mM (*S*)-α-FMT. Most crystals diffracted poorly; however there was one crystal that provided a full data set at 2.8A. Using a BLAST alignment search against the Protein Databank, homologous protein structures suitable for molecular replacement were identified. All putative structures had

less than 30% sequence identity with CLOSPO_02083 and the top 5 hits, measured by e-value (3F9T, 3MBB, 3MAF, 3MAU, 3MAD), were used to generate an ensemble search model by *Phenix.ensembler.* Further modification of the input search structures was performed using *Phenix.sculptor* and all phasing attempts were performed using *Phaser* (University of Cambridge).

Unfortunately, there was no molecular replacement solution. The next step was to purify in the presence of seleno-methionine to increase the resolution and provide sufficient data to solve the structure. While adequate amounts of protein were obtained from a Se-Met purification and crystals grew under similar conditions (0.1M citrate pH 5 and pH 5.25, 30-40% ethoxyethanol, 40% polypropylene glycol P400 or 0.1M ATP), they were not of high enough quality to obtain a full data set (small, hollow-looking rods). Were this project to continue, the next best step would be to screen a Se-Met preparation of the enzyme in the presence of (*S*)-α-FMT against the JCSG CORE Suites.

Crystallization of ligand bound RUMGNA_01526

The JCSG CORE screen was used with purified RUMGNA_01526 (new construct that had a shorter linker between the tag and N-terminus of protein) and (*S*)-α-FMT by pre-mixing protein and ligand before adding to the well. Crystals were observed in the following conditions:

(1) 0.2M disodium tartrate dihydrate, 20% PEG 3350

(2) 0.2M potassium sodium tartrate tetrahydrate, 20% PEG 3350

(3) 0.1M Bicine pH 9, 40% MPD

(4) 0.1M Tris pH 8.5, 20% PEG 1000

(5) 0.2M tri-potassium citrate monohydrate, 20% PEG 3350

(6) 0.2M trisodium citrate dihydrate, 20% PEG 3350

(7) 0.2M potassium citrate, 20% PEG 3350

(8) 0.2M lithium citrate, 20% PEG 3350

Optimization was performed around conditions (1), (2), (4) and (4) with PEG 3350 instead of PEG 1000, (6), and (7). Crystals were observed after three days in several conditions but the following were chosen for freezing with 10% glycerol:

(9) 0.1M Tris pH 8, 22.5% PEG 3350

(10) 0.2M disodium tartrate, 17.5% PEG 3350

(11) 0.2M potassium sodium tartrate tetrahydrate, 17.5% PEG 3350

(12) 0.2M trisodium citrate, 20% PEG 3350

(13) 0.2M potassium citrate, 20% PEG 3350

The best diffraction was collected from crystals in condition (13). The ligand bound structure revealed an allosteric binding site (discussed below). This raised the possibility that the active site substrate specificity could be controlled allosterically. A structure with a stronger (tryptophan) or weaker (phenylalanine) affinity substrate would enhance our understanding of how this allosteric site affected the active site. Crystal trays were set up in three conditions (0.1M Bicine pH 8.5/25% PEG, 0.2M potassium citrate/20% PEG 3350, and 0.1M Tris pH 8/22.5% PEG 1000) in the presence of tryptophan or phenylalanine. While some crystals did form, none were suitable for crystallography.

Structure of ligand bound RUMGNA_01526

We determined the crystal structure of inhibitor-bound RUMGNA_01526 at 2.8 Å. The major difference between the native and (*S*)-α-FMT-bound structures is the conformation of an extended loop (residues 337-349). The homologous loop was previously identified as a major difference between GAD65 and GAD67, where differences in conformational dynamics are thought to be responsible for auto-inactivation of GAD65 (40). In porcine DOPA decarboxylase, this loop was disordered in three data sets from complexes with different inhibitors, complicating structure-based drug design and an assessment of catalytic mechanisms (46). In contrast, we observed that when bound to PLP alone, this loop was partially disordered and the remaining ordered components jutted away from the active site, leaving the active site solvent-exposed. Upon engagement of (*S*)-α-FMT, electron density became clearer and the loop folded over the active site, excluding solvent and forming critical interactions with the inhibitor (Figure 3.7D). These data are consistent with a model in which loop 337-349 gates the active site, adopting a partially disordered, outward-facing conformation in the absence of substrate that enables access to the active site, and closing down to cap the active site after substrate entry.

Two other flexible loops within the active site of the inhibitor-bound enzyme are reordered to accommodate the indole side chain of (*S*)-α-FMT. In the absence of substrate, the first loop (residues 95-101) leaves the active site accessible for the entry of a substrate with a large aromatic side chain. Upon substrate binding, the loop conformational change places the phenyl ring of Phe98 directly above the p-system of the indole ring, stabilizing the inhibitor through a p-stacking interaction (Figure 3.7C). This

loop appears to be a critical element for defining substrate selectivity; consistent with this possibility, it is conserved among decarboxylases in several related Firmicutes (discussed below). The second loop, residues 329-336, reorients to shift the phenolic side chain of Tyr335 closer to the active site, increasing the hydrophobicity of the substrate-binding pocket.

Figure 3. 7

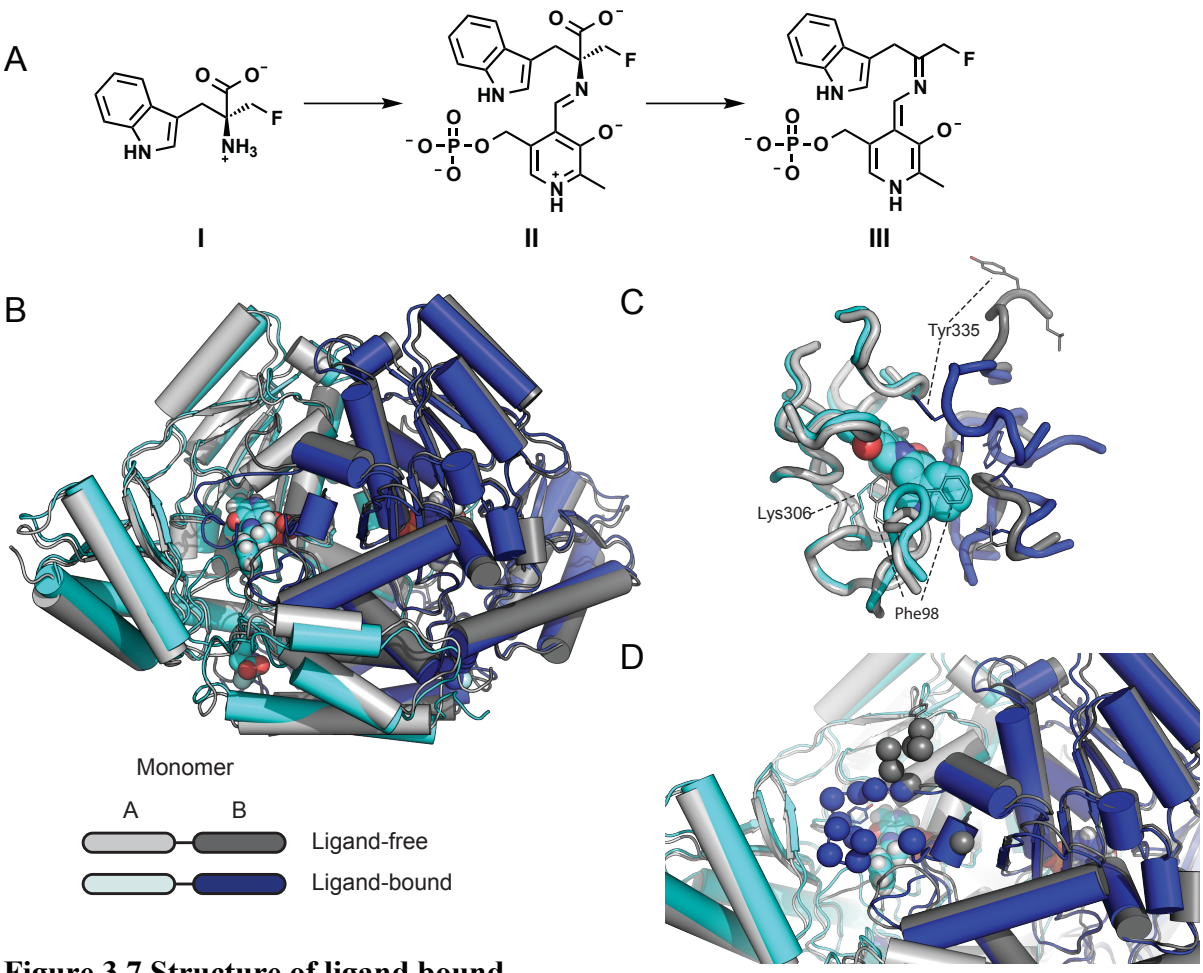

Figure 3.7 Structure of ligand bound

RUMGNA_01526 A) Schematic of proposed inhibitor mechanism: (*S*)-α-FMT (**I**) is converted to a PLP-(*S*)-α-FMT external aldimine intermediate (**II**), which is decarboxylated to a PLP-(*S*)-α-FMT Schiff base adduct (**III**). (B) Overlay of ligand-free (monomer A, light gray and monomer B, dark gray) and ligand-bound (monomer A, cyan and monomer B, blue) structures. In the active and allosteric sites, PLP-(*S*)-α-FMT and (*S*)-α-FMT (respectively) are shown in spheres. (C) Active site with PLP-(*S*)-α-FMT bound reveals a repositioning of Tyr335 and Phe98. In the ligand-bound structure,

Lys306 is no longer covalently bound to PLP. (D) Upon engagement of (*S*)-α-FMT, residues 337-349 (dark blue spheres) fold over the active site, excluding solvent and forming critical interactions with the inhibitor. Dark gray spheres represent only ordered residues in apo structure.

In the inhibitor-bound structure, (*S*)-α-FMT has been decarboxylated; however, it has not been defluorinated as seen in the mechanism of (*S*)-α-FMH inhibition of histidine decarboxylase, and remains covalently linked to PLP. This is supported by the absence of a suitable nucleophile in the active site that could be covalently modified by the defluorinated (*S*)-α-FMT-PLP adduct.

The (*S*)-α-FMT-PLP adduct (Figure 3.7A, **III**) is relatively disordered in the electron density maps of both active sites, and the maps show an absence of density consistent with a covalent linkage between PLP and the enzyme. Collectively, these data indicate that the (*S*)-α-FMT has not been defluorinated; rather, a PLP-(*S*)-α-FMT adduct is formed and remains tightly bound rather than diffusing out of the active site. Thus, the blockade of RUMGNA_01526 by (*S*)-α-FMT appears to be an enzyme-catalyzed inactivation of the PLP coenzyme, and does not involve a chemical modification of the enzyme itself.

Surprisingly, we observed an additional molecule of (*S*)-α-FMT bound to a site ~20 Å from the active site (Figure 3.8A). The inhibitor fits inside a hydrophobic pocket that is formed by the movement of an N-terminal loop (residues 16-22) and makes hydrogen bonds to S105 and the backbone of P102. While this binding event might be a crystallization artifact, the kinetic data are consistent with the possibility of cooperative substrate binding to an allosteric site as evidenced by a slight increase in the r^2 value for the fit to the Hill equation (Hill coefficient = 1.87) versus the Michaelis-Menten equation (Figure 3.8B,C).

Figure 3. 8

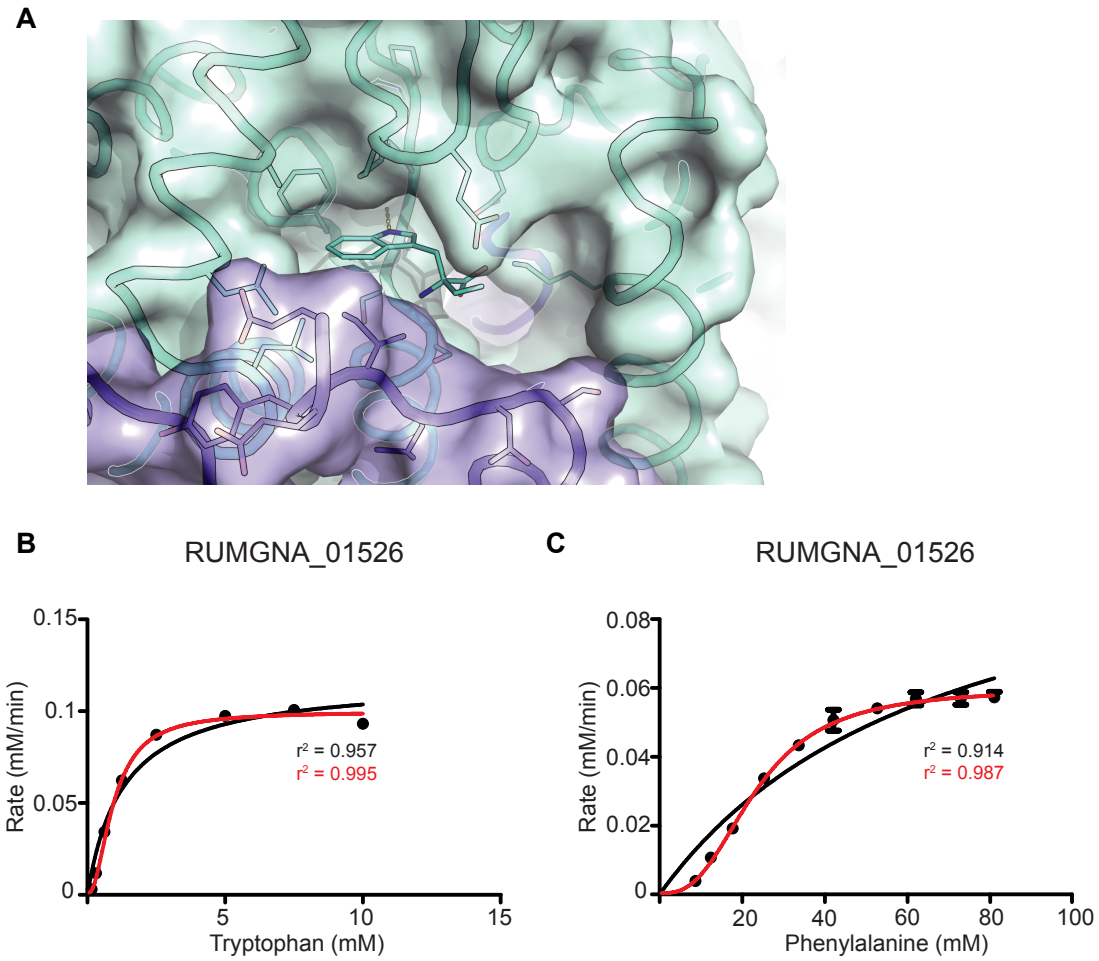

Figure 3. 8 Structure of allosteric binding site in RUMGNA_01526 (A) Allosteric site shows free (*S*)-α-FMT buried in a hydrophobic pocket near the N-terminus of the enzyme. Hill equation fit to RUMGNA_01526 kinetic data. Rate (mM tryptamine/min) vs substrate concentration curves for (B) tryptophan or (C) phenylalanine decarboxylation by RUMGNA_01526. GraphPad was used to fit the Michaelis-Menten (black) and Hill (red) equations.

Table 3. 1 Data collection and refinement statistics

	Apo-RUMGNA_01526	S-α-FMT-RUMGNA_01526
Wavelength (Å)		
Resolution range (Å)	79.37 - 2.804 (2.905 - 2.804)	52.44 - 2.84 (2.942 - 2.84)
Space group	P 1	P 41 21 2
Unit cell	58.63 145.77 165.07 72.85 88.84 88.3	135.03 135.03 249.8 90 90 90
Total reflections	218936 (22174)	730528 (73919)
Unique reflections	121102 (12262)	55248 (5448)
Multiplicity	1.8 (1.8)	13.2 (13.6)
Completeness (%)	94.70 (96.28)	99.97 (99.96)
Mean I/sigma(I)	9.54 (2.09)	25.80 (3.80)
Wilson B-factor	41.16	54.76
R-merge	0.08033 (0.363)	0.119 (0.8652)
R-meas	0.1136	0.1238
CC1/2	0.99 (0.73)	0.999 (0.881)
CC*	0.998 (0.919)	1 (0.968)
R-work	0.2311 (0.3077)	0.2098 (0.2745)
R-free	0.2568 (0.3623)	0.2423 (0.3494)
Number of atoms	29598	15146
macromolecules	29064	14886
ligands	120	184
water	414	0
Protein residues	3696	1889
RMS(bonds)	0.002	0.007
RMS(angles)	0.67	0.64
Ramachandran favored (%)	96	95
Ramachandran outliers (%)	0	0.053
Clashscore	3.03	3.04
Average B-factor	21.2	36.4
macromolecules	21.3	36.2
ligands	41.8	47.9
solvent	9.7	

Statistics for the highest-resolution shell are shown in parentheses.

Data collection and refinement performed by Andrew Van Benschoten

Experimental Procedures

Protein purification

E. coli BL21(DE3) containing pET28a+RUMGNA_01526 was grown in LB medium with kanamycin (50 μg/mL) at 37C. At OD_{600} of 0.6-0.8 1mM IPTG was added and the temperature reduced to 25C. Cells were grown overnight and harvested by centrifugation. Cell pellets were resuspended in 50 mM NaH_2PO_4 pH 8.0 300 mM NaCl, 10mM imidazole with proteosome inhibitors (EDTA free, Roche). Cells were lysed using a C3 emulsiflex for 10 minutes at 15000 psi and cell debris was removed by centrifugation at 16000rpm for 20 minutes. Supernatant was applied to Qiagen Nickel-NTA agarose beads (1.5 mL beads/L culture) and incubated at 4C for 1 hour. Beads were centrifuged at 1000 rpm for 2 minutes and washed in 100 mM NaH_2PO_4 pH 8.0, 300 mM NaCl, 20 mM Imidazole. Enzyme was eluted with 3 mL of 50 mM NaH_2PO_4 pH 8.0, 300mM NaCl, 250mM Imidazole and dialyzed against 50mM Tris pH 7.5, 300mM NaCl (Thermo Scientific, Slide-A-Lyzer 20K dialysis cassette). For the ligand-free structure of RUMGNA_01526, enzyme was FPLC purified and fractions were collected and concentrated. For kinetic studies and the ligand-bound structure, no FPLC was performed. When purifying CLOSPO_02083, 30 μM PLP was added to the LB culture media during expression. Additionally, 10 mM tryptophan and 30 μM PLP were added to the lysis buffer and 30uM PLP was added to the dialysis buffer.

Crystallography

Purified proteins were screened against the JCSG CORE Suite in 96 well sitting drop plates at 10 mg/mL. Conditions that produced crystals were optimized in 15-well hanging drop plates with 500 uL well solution. For ligand-bound conditions, (*S*)-α-FMT was pre-incubated with the enzyme at various concentrations before mixing with crystallographic solution.

Crystals of RUMGNA_01526 were grown at room temperature in hanging drops consisting of equal volumes (1 + 1 μl) of 10 mg/ml RUMGNA_01526 and a crystallization solution composed of 0.1 M Bicine pH 8.5 and 25% PEG 3350. Crystals of RUMGNA_01526 with (*S*)-α-FMT were grown at room temperature in sitting drops consisting of equal volumes of 10 mg/mL RUMGNA_01526 pre-mixed with 5 mM (*S*)-α-FMT and a crystallization solution composed of 0.2 M potassium citrate and 20% PEG 3350.

Structure Determination and Refinement

Crystals were flash-frozen in liquid nitrogen with 10% glycerol supplemented as a cryoprotectant. Data were collected on beamline 8.3.1 at the Advanced Light Source (Table 3.1). X-ray reflections were processed using xia2. All subsequent molecular replacement and structure analysis was performed using the PHENIX software suite. For the apo-structure, a molecular replacement search ensemble was created from the homologous models 2JIS, 3RBF, 4E1O, 3RCH, 2QMA and 1JS3 using Phenix.sculptor and Phenix.ensembler. The solved apo-enzyme structure was used as a molecular

replacement search model for the inhibitor-bound structure. All visualization components were performed using COOT.

Kinetic analysis

Purified enzyme was used to determine the catalytic efficiency (k_{cat}/K_m). 20 nM of RUMGNA_01526 was incubated with 0.15-10 mM tryptophan in 50 mM sodium phosphate pH 6.5, 300 mM NaCl, 40 μM PLP at 37C for 7 min. Reactions were quenched with equal volume MeOH and 100 μL was injected onto the HPLC for analysis. A standard curve was used to determine rate of tryptamine production. Under the same buffer conditions, 500 nM of RUMGNA_01526 was incubated with 5-80 mM phenylalanine for 10 minutes and 100 nM of CLOSPO_02083 was incubated with 0.15-24.5 mM tryptophan for 6 minutes. Triplicate measurements made from one batch of purified enzyme.

Covalent inhibition of S-α−fluoromethyltryptamine was measured by analyzing product formation over time after addition of inhibitor to pre-incubated enzyme and substrate at a concentration of $3K_m$. Progress curves were fitted to the equation $[P]=(v_i/k_{obs})(1-\exp(-k_{obs}t))$, where P is the product formed at time t, v_i is the initial velocity, and k_{obs} is the apparent first-order rate constant for enzyme inactivation. The k_{obs} were plotted verses inhibitor concentration and fitted to the equation $k_{obs}=k_{inact}[I]/(K_{app}+[I])$, where K_{app} is the apparent dissociation constant of the reversible enzyme-inhibitor complex, and k_{inact} is the first-order rate constant for apparent irreversible conversion of the enzyme-inhibitor complex to covalently bound complex.

K_i values were calculated using the equation $K_i=K_{app}/(1+[\text{tryptophan}])/K_{mTRYPTOPHAN})$ using experimentally determined K_m values for tryptophan (47).

Chapter 4—Characterizing the *in vivo* production of tryptamine

Introduction

Discovering the production of tryptamine and related biogenic amines by human gut colonizing bacteria begs the question: how do these molecules influence host physiology and behavior? It has long been hypothesized that the gut influences the brain, but no molecular mechanism as been elucidated.

We were interested in whether bacterially produced tryptamine could be influencing host intestinal epithelial cell function. In order to determine the role of tryptamine-producing microbes, we intended to generate a knockout strain of bacteria that would allow for the most direct comparison. By colonizing mice with a wild type or knockout strain, we could begin to evaluate the difference that tryptamine is playing in host physiology and behavior.

Generating a knockout in either *C. sporogenes* or *R. gnavus* proved to be very challenging. A handful of genetic knockouts have been generated in *Clostridium* species using the ClosTron system (described below) (48). However, to our knowledge there has never been a published knockout in *Ruminococcus*. Our strategy was to attempt a knockout in *C. sporogenes*, but also to knock-in the decarboxylase from *R. gnavus* into a wild type strain of *E. coli* that would create a matched pair of strains in order to do a preliminary evaluation in mice.

Tryptamine is relatively understudied as it relates to host physiology. However, we know that it is an agonist of serotonin receptors. Over 90% of human serotonin is produced in intestinal enterochromaffin cells. Serotonin regulates several aspects of gastrointestinal function with the most characterized being the ability to regulate motility (49). Therefore, as an initial experimental condition, we evaluated GI motility in mice containing only *E. coli* MG1655 with either a vector control plasmid knocked in, or the tryptophan decarboxylase from *Ruminococcus gnavus*.

Results and Discussion

C. sporogenes knock-out strategy and attempts

ClosTron is the primary system used to modify the genome of *Clostridium* species (48). It exploits the mobile group II intron from *Lactococcus lactis* that integrates a self-slicing mobile element into a targeted DNA site (50). The mobile element contains an antibiotic resistance marker that is only activated post-integration after self-splicing of an internal group I element. Once the intron has been re-targeted for the gene of interest, it is introduced into the *Clostridium* species by conjugation with an *E. coli* donor strain. This system has been used to make several knockouts in various *Clostridium* species including *C. sporogenes*. Targeting of the specific DNA site in the genome involves three separate regions within the intron. The creators of ClosTron designed a web-based tool that generates a list of target sequences and evaluates their probability of success. We successfully constructed 7 different plasmids using these algorithms and although conjugation was successful of each of these plasmids, we were never able to produce a

single or double crossover mutant. The list of target sequences attempted is provided below.

We attempted to use the ClosTron system on multiple occasions. The first set of experiments resulted in conjugation that generated small, hard white colonies that were difficult to re-streak. The colonies that did re-streak had the right antibiotic resistance profile, but in the screening process we did not see any plasmid integration. This could have been due to spontaneous erythromycin resistance so we started adding lincomycin to prevent this from happening. The second round of experiments resulted in several "wet" *E. coli* looking colonies growing out of the "sludge" of conjugation. These colonies had the correct antibiotic resistance profile; however, they did not possess the characteristic phenotype of *C. sporogenes* colonies from previous attempts, and still contained the intact decarboxylase gene.

After several rounds of ClosTron failed, we also attempted a brute force method by trying to achieve a gene disruption. We constructed a plasmid (pHY304) that contained ~1kB of *matching* sequence to the decarboxylase and electroporated the plasmid at high concentrations into *C. sporogenes* (51). Although the bacteria survived electroporation (as evidenced by growth on antibiotic free plates), no antibiotic resistant colonies resulted. This strategy was only attempted once without detailed troubleshooting. In the future, optimizing the amount of DNA in the electroporation as well as settings on the instrument might yield better results.

The lack of success does not seem to have a worthy justification. Going forward, it may be worthwhile to PCR the gene and confirm that the sequence matches the one

used to generate the target sites as this system relies on the specific nucleic acid sequence of three short regions within the gene and sequence variation can occur between strains. Generating a knockout of this gene will most likely involve the construction of several (>10) plasmids with different target sequences, possibly in different ClosTron plasmids, and a systematic assessment of each. While it is possible, it will involve extreme time and effort.

Table 4. 1

Sequence	Exon--><--Exon	Pos	Score
GGTTCCGTAGATGATCCAGATTTATATGCTAATATTTTTGATAAA		645|646s	10.235
CTTAATGGAAATGATGAAGAATTTGATGGATATGTAACTCAGGGA		321|322s	6.808
AGCTATATGGATGGTACTTGCTAGCTACGGACCATATGGATGGAT		956|957s	6.746
TTAAATATAGATATAATAAAAGTTCCAGTAGATTTTTACAGTCGT		501|502s	6.630
AAGATAGTCGTTATGGAACATGTTGAATTAGATATATTAAATTCC		1188|1189s	6.449
GGATATGTAACTCAGGGAGGAACCGAAGCTAATATACAAGCTATG		348|349s	6.169
TATCCTATAGATAATAAAGAGTGTAAAACGGATTTTTCTAATAAA		741|742s	5.949
ACTAAATTGGATGATACTGTTTTTTATGACGATCATAGCTTTGTA		138|139s	5.620
ATCCATATAGCTACAGCATTAGAACCTGAGCGGCTACCACTTAGC		908|909a	5.465
AGCTTCTTTGACAATGCTATCTAAAGTGTTCTCTTGAATTTTACG		528|529a	5.438
CAATATGTTAATAAAGAAATAGCAGAAAAATACTTCCTGGTACCA		1113|1114s	4.943
AAAATTCATGTTGACGGAGCTTTCGGTGGATTCATATATCCTATA		705|706s	4.698
AATATTTTTGATAAATATAATTTAGAATATAAAATTCATGTTGAC		675|676s	4.633
TATGATTTGGATTTTGTATAAATGTTCTTAGATATGGTGAGTGCT		169|170a	4.261
GGAACCTTTGATATAGAAAGAGAGCTCATTCAATTATTAGCAATT		270|271s	4.176
TATAAAATTCATGTTGACGGAGCTTTCGGTGGATTCATATATCCT		702|703s	4.029
TTTAAAAAAGAAAGAAAAGCAAAACATGAGGAAATAGCTATAATC		411|412s	3.967
GTCAAAGAAGCTAAAGAAATTGGGAAAAAATATTTTATAGTAATA		576|577s	3.638
CATCATTTCCATTAAGAACATCAATTGCTAATAATTGAATGAGCT		277|278a	3.375
AGTTACTATGTTCATACTGTCCTCTTTGTAATATTTAATTCTCAT		1044|1045a	3.249
GTTGACGGAGCTTTCGGTGGATTCATATATCCTATAGATAATAAA		714|715s	3.026
ACTCTTACAAAGGAAGCAACTTATATAGAGAATTTAGATGTTACG		879|880s	2.948
ATTCATGTTGACGGAGCTTTCGGTGGATTCATATATCCTATAGAT		708|709s	2.736
GCAATTGATGTTCTTAATGGAAATGATGAAGAATTTGATGGATAT		309|310s	2.675
GAATTTTACGACTGTAAAAATCTACTGGAACTTTTATTATATCTA		493|494a	2.558

Table 4.1 Results of clostron intron design tool. The target sites highlighted in the red box were selected for cloning into pMTL007C-E2

Lactobacillus brevis knockout

Although our primary interest was to study the effects of tryptamine, we also were interested in tyramine. It is known that tyramine is capable of regulating blood pressure and it would be interesting to know whether the gut microbiome was producing molecules that influenced heart rate. To do this, we used the pMAD plasmid to insert a resistance marker into the tyramine decarboxylase we identified in *Lactobacillus brevis* (52). Initial attempts at gene disruption were highly successful, where greater than 50% of colonies screened were positive for gene disruption (See Figure 4.1 for knockout schematic). The mutant phenotype was confirmed by incubating stationary phase bacteria in minimal media containing tyrosine. After 24 hours, the tyrosine remained in the absence of tyramine.

Figure 4. 1

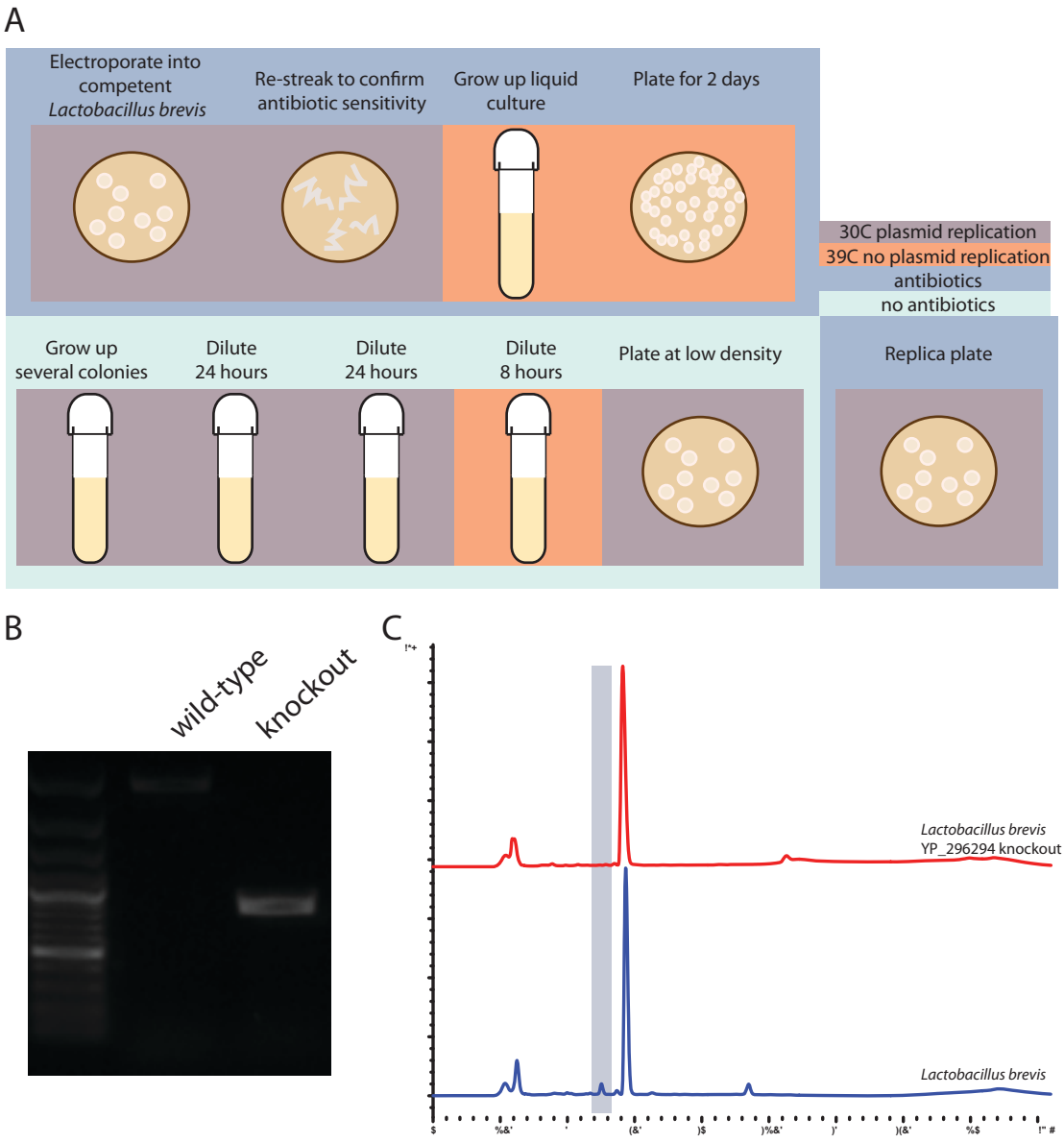

Figure 4.1 ***Lactobacillus brevis*** **knockout**. (A) Schematic of protocol to generate knockout. (B) PCR confirming knockout. Wild-type strain PCR product (very faint band) is ~1.5kB larger than knockout strain. (C) After confirming knockout by PCR, mutant and wild type strains were grown overnight and transferred to minimal media containing tyrosine. The mutant is no longer able to produce tyramine.

RUMGNA_01526 knock-in to E. coli

Because our attempts to knockout tryptophan decarboxylase in *Clostridium sporogenes* failed, we decided to knock the gene into a wild type *E. coli* strain for *in vivo* studies. Although this was not the perfect system, it would allow us to evaluate the potency of tryptamine produced by commensal gut bacteria. We chose to work with the decarboxylase from *R. gnavus* because it was more active and we had bioinformatic data suggesting that more humans are colonized with *R. gnavus* than *C. sporogenes* (work by Laurens Kraal, not yet published).

We employed the CRIM (conditional-replication, integration and modular plasmids) system to insert the decarboxylase into the *E. coli* chromosome (53). This system allows for insertion of a gene of interest into a phage attachment site within the *E. coli* genome. This simple strategy employs a plasmid carrying a phage attachment site homologous to one in the *E. coli* genome. A helper plasmid is transferred with the integration plasmid carrying the gene for the phage integrase protein, which assists in integrating the entire plasmid. We selected the pAH70 plasmid to integrate into the HK022 site, which contained a synthetic constitutive promoter and kanamycin resistance gene. Once RUMGNA_01526 was cloned into pAH70, the plasmid was transformed into *E. coli* MG1655 cells that contained a helper plasmid. This method worked to generate the knock-in after one attempt. The phenotype was confirmed by performing the *E. coli* assay described in Chapter 2.

Figure 4. 2

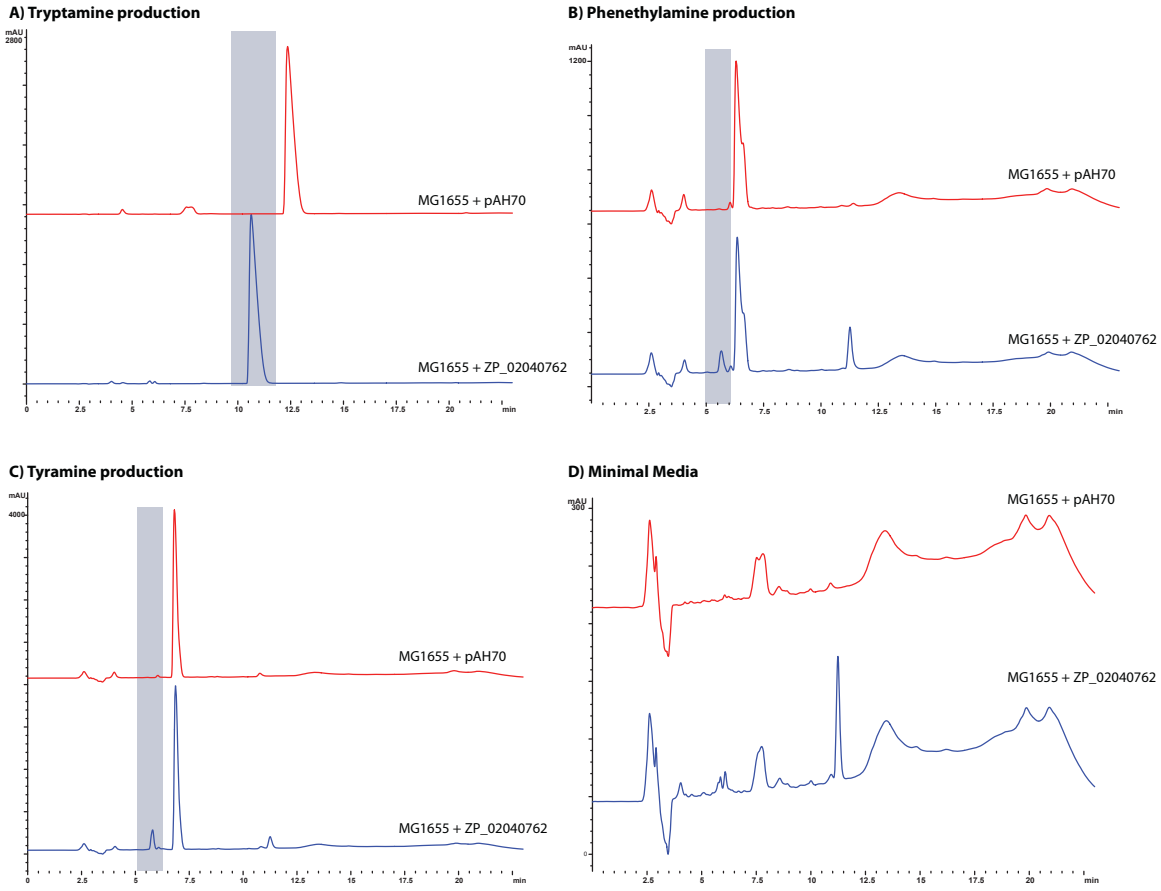

Figure 4.2 *E. coli* MG1655 stably integrated with RUMGNA_01526 produces tryptamine. Colonies sequenced for positive integration of RUMGNA_01526 were fed (A) tryptophan, (B) phenylalanine, (C) tyrosine, or (D) minimal media alone. After 24 hours, cell free supernatant was analyzed by HPLC. The mutant *E. coli* is capable of decarboxylating all three substrates, but is most efficient producing tryptamine.

In vivo study design

Because it is known that tryptamine can induce serotonin release from enterochromaffin cells and that increased levels of serotonin induce diarrhea, we were expecting to see a difference in GI motility between the vector control and decarboxylase containing *E. coli* strains (54). To boost the signal from tryptamine, we tried introducing tryptophan into the chow, as well as administering a monoamine oxidase inhibitor that would increase the half-life of tryptamine. The time course of the experiment is described in Figure 4.3.

Figure 4. 3

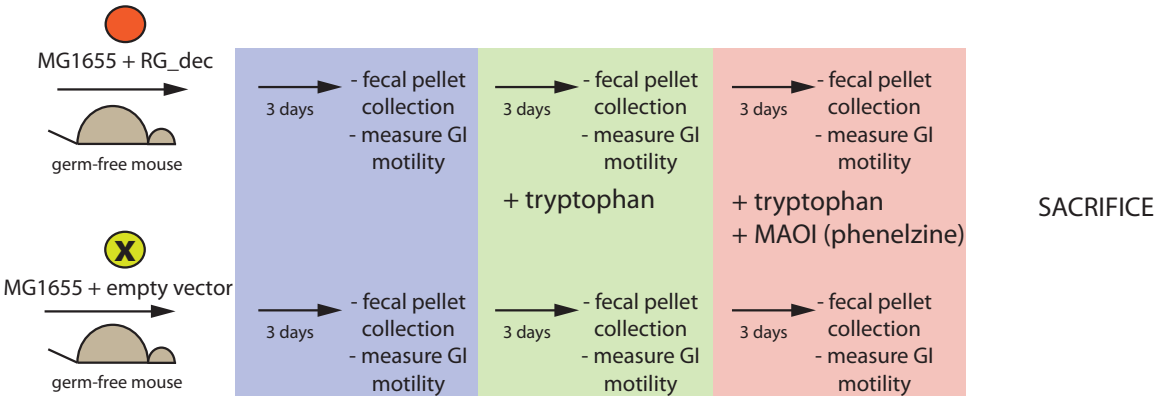

Figure 4.3 *In vivo* study design. Germ-free mice were gavaged with *E. coli* MG1655 expressing either RUMGNA_01526 or a vector control. Fecal samples were collected and GI motility measurements were performed after 3 days, as well as after tryptophan feeding and tryptophan plus a monoamine oxidase inhibitor treatment.

Colonization confirmation by E. coli MG1655 mutant strains

In collaboration with Justin Sonnenburg at Stanford, germ-free mice were colonized with *E. coli* that contained either an inactive enzyme (vector control, from the pAH70 plasmid) or the *R. gnavus* tryptophan decarboxylase. Colonization was confirmed by performing PCR on DNA extracted from fecal pellets using primers specific to either the decarboxylase or the vector (Figure 4.4).

Figure 4. 4

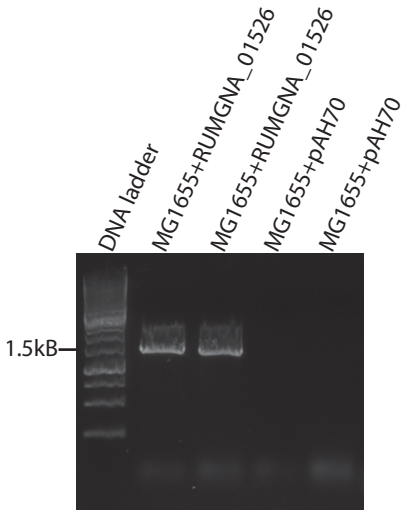

Figure 4.4 Colonization of *E. coli* MG1655 vector control and RUMGNA_01526 strain. Fecal DNA was prepared using the Zymo Fecal Pellet MiniPrep kit and used in a PCR reaction with primers specific for RUMGNA_01526. This confirms the vector control mice did not express any tryptophan decarboxylase.

GI motility measurements

To test the hypothesis that bacterially produced tryptamine influenced GI motility, we administered a red dye in the drinking water and measured the rate of excretion. The GI motility time varied from 250 to 400 minutes. In every condition, we observed similar transit times between mice colonized with *E. coli* containing the vector control or decarboxylase.

Figure 4. 5

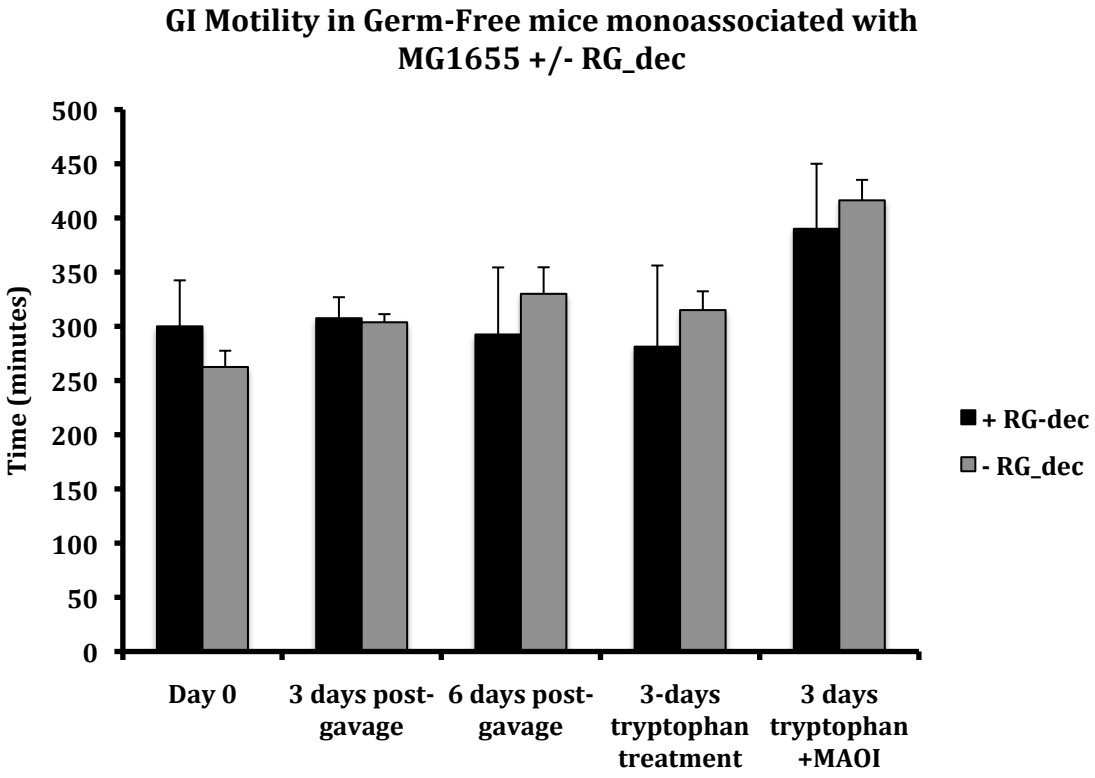

Figure 4.5 GI motility measurements. Transit time (in minutes) of a red dye was measured in both cohorts of mice every three days. Average of four mice is presented. Error bars represent standard error of the mean.

Quantification of tryptamine and 5-HIAA in mice colonized with E. coli MG1655 mutants

Although we did not see any physiological differences between the two cohorts of mice, we were interested in measuring the levels of tryptamine produced. To do this, we performed an organic extraction of fecal pellets collected at each time point of the experiment. Using LC/MS/MS we analyzed the extracts for both tryptamine and 5-hydroxyindoleacetic acid (the primary serotonin metabolite).

We saw a noticeable difference in tryptamine at each time point of the experiment. This suggests that tryptamine levels in the intestine are maintained without dietary supplementation or metabolism inhibition. It could be that intestinal tryptamine is not subject to oxidation by mono-amine oxidases, or that these enzymes are not expressed at high levels in the intestine. It would be interesting to measure the levels of tryptamine and tryptophan in the blood. If there were more tryptamine and/or less tryptophan in the plasma of mice colonized with *E. coli* expressing the tryptophan decarboxylase, this would indicate the possibility of systemic effects. The MAOI treatment would also be more likely to show an effect in the plasma as that is where it is primarily known to function.

However, we did not see a difference in the levels of 5-HIAA. Together with the GI motility data, this could indicate that the tryptamine is not inducing a *large* release of serotonin.

Figure 4. 6

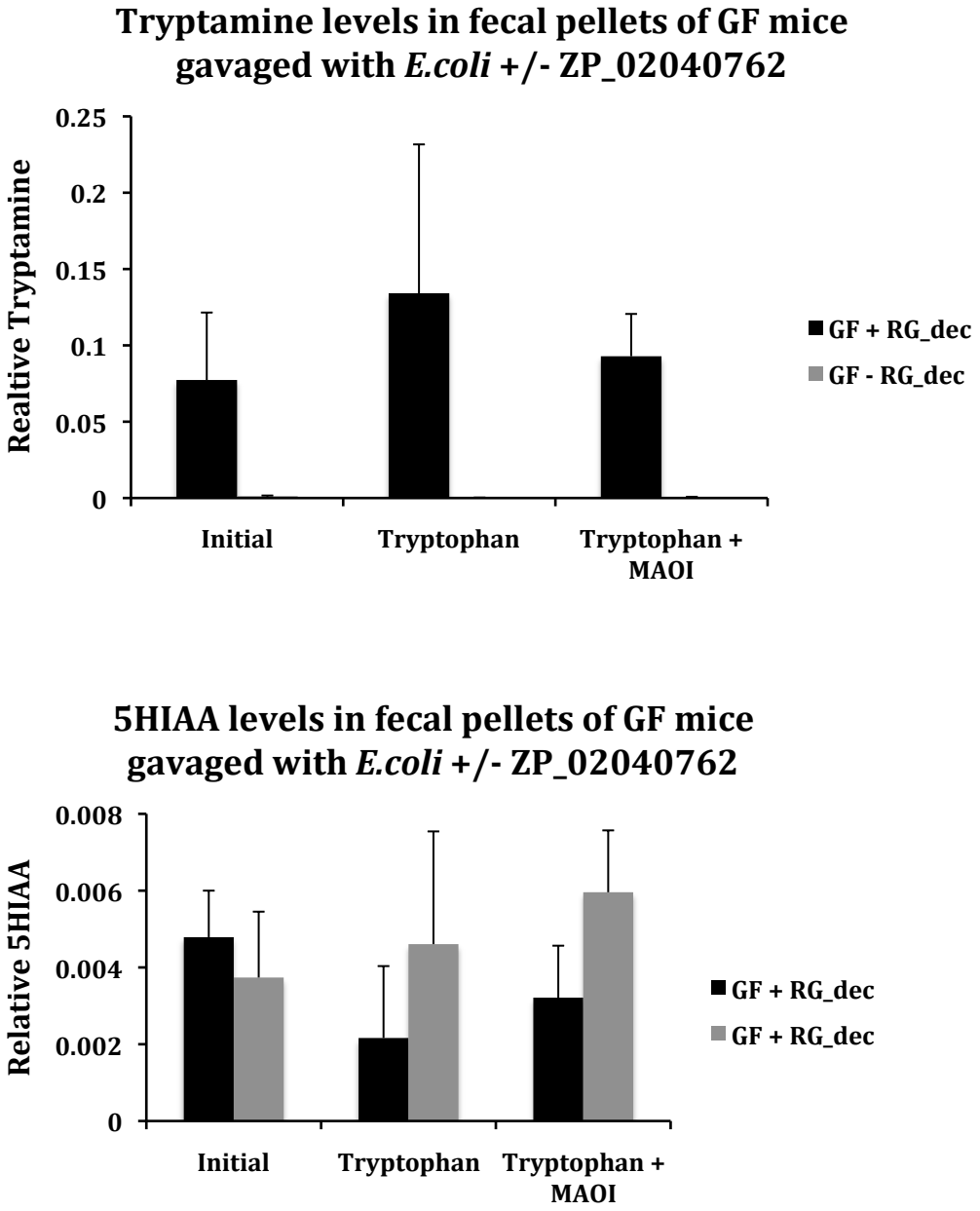

Figure 4.6 Levels of tryptamine and 5-HIAA in fecal pellets. LC/MS/MS was used to analyze the levels of tryptamine and 5-HIAA. A program was used to specifically identify tryptamine and 5-HIAA in two different runs. Tryptamine and 5-HIAA are presented relative to an internal control of dinitrobenzene.

Quantification of tryptamine and 5-HIAA in fecal pellets of mice colonized with C. sporogenes

Although we were not able to produce a decarboxylase knockout strain of *C. sporogenes*, we were still interested in understanding whether the strain would produce tryptamine in the gut. We took advantage of the fact that we had fecal samples from a previous experiment of mice monoassociated with *C. sporogenes* or biassociated with *C. sporogenes* and *B. thetaoitamicron*.

We analyzed the levels of tryptamine and 5-HIAA in mice monocolonized with *C. sporogenes* or *C. sporogenes* plus *B. thetaiotamicron* by LC/MS/MS. All samples contained tryptamine. Compared to mice colonized with the *E. coli* vector control, there are elevated levels of tryptamine. However, there is less tryptamine than observed in the *E. coli* expressing RUMGNA_01526. This could be due to the fact that RUMGNA_01526 is a more active enzyme than CLOSPO_02083. In future experiments, it would be important to include more controls of mice monoassociated with strains not known to produce tryptamine. While this was a small study of only a few mice, if the results repeated in a larger study, it could verify that specific strains of the gut microbiota are contributing to the intestinal pool of tryptamine. This would also indicate that the gut microbiota are depleting the tryptophan available to the host to perform other functions, such as crossing the blood brain barrier to participate in serotonin synthesis.

Figure 4. 7

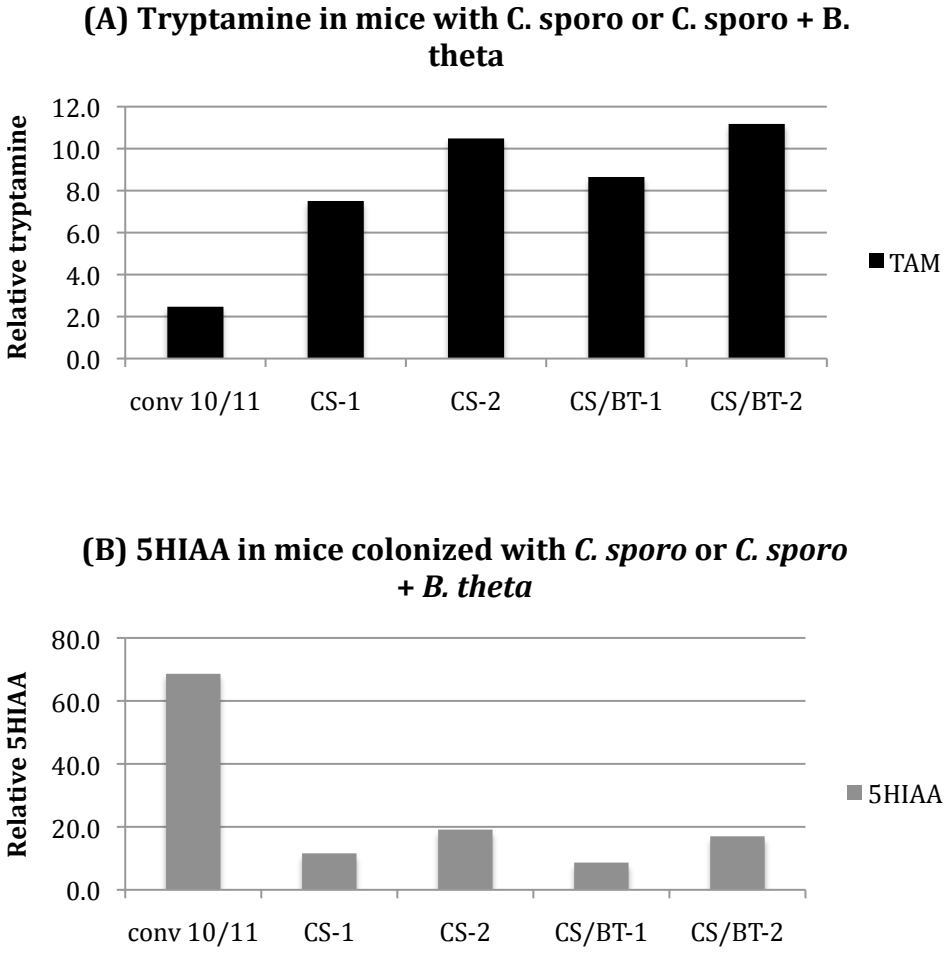

Figure 4.7 Fecal tryptamine and 5-HIAA levels in mono- and bi-associated mice. (A) Tryptamine and (B) 5-HIAA were measured in the fecal pellets of mice monoassociated with *C. sporogenes* (CS-1, CS-2) or bi-associated with *C. sporogenes* and *B. thetaiotamicron* (CS/BT-1, CS/BT-2). There is not a noticeable difference between the two colonization states; however there is a slight difference when compared to a conventional mouse.

Experimental Procedures

ClosTron

The first step is to redesign the Ll.LtrB intron to target the tryptophan decarboxylase. Using the algorithm provided on www.clostron.com, we selected several targets with the highest probability of success (provided in Table 4.1 above). This involves mutating three separate regions within the ~350bp intron. Using Splicing by Overlap Extension (SOE) PCR, the intron was constructed with the unique target sequences. The first three introns were constructed successfully by Mao Taketani. However, during the second round of intron development, only two of the three target regions were successfully mutated. We determined it was a better use of our time to have the new introns synthesized and cloned into the pMTL007C-E2 plasmid by DNA2.0.

Once the retargeted plasmids were constructed, they were transformed into a conjugation donor strain of *E. coli* HB101. Overnight cultures of *E. coli* HB101 harboring pMTL007C-E2+trp_dec_KO plasmids were diluted and grown to a density of 0.8 before being pelleted and resuspended in a saturated culture of *C. sporogenes*. It was important to resuspend gently (and under anaerobic conditions) to ensure the integrity of the donor strain. Resuspended cultures were spotted in 50 μL aliquots on antibiotic free TYG plates and incubated anaerobically overnight. After ~20 hours, cells were scraped and resuspended in 1 mL TYG media and plated across 5 TYG plates containing 10 μg/mL thiamphenicol, 250 μg/mL D-cycloserine, and 50 μg/mL kanamycin to select for *C. sporogenes* harboring the pMTL007C-E2 plasmid. Small, hard, white colonies generally appeared after 5 days. These colonies were restreaked on TYG+10 μg/mL thaimphenicol to confirm plasmid transfer. Any colonies appearing on these plates were

restreaked on TYG+erythromycin+lincomycin to select for integration. Using both erythromycin and lincomycin prevented spontaneous generation of resistance. Colonies appearing on these plates were analyzed by PCR for gene disruption.

E. coli knock-in

RUMGNA_01526 was PCR amplified using primers with 25nt overlap with the pAH70 plasmid from the CRIM system. A CPEC reaction was performed to ligate the gene into the plasmid (after digest with NdeI and BamHI to remove pstS*), and 3 μL of this reaction was chemically transformed into competent MG1655 cells carrying the pAH69 helper plasmid. Emergent colonies were sequenced and a positive clone was selected for further experiments. To create a control construct, unmodified pAH70 plasmid (including an inactive enzyme) was integrated into MG1655.

Lactobacillus brevis knock out

The thermosensitive plasmid pMAD was used generate a YP_296294 *Lactobacillus brevis* knockout strain. ~1kB of sequencing flanking the gene both up and down stream was amplified and ligated by PCR and cloned into the pMAD vector using CPEC (described in Chapter 2). An overnight culture of *L. brevis* was diluted 1:10 into fresh MRS and grown to OD 0.6. The cells were washed three times in 20 mL SM, and resuspended in 100 μL SM. 2 μL of EB or plasmid was added and the mixture electroporated (2kV, 3.8-3.9 ms). 900 μL fresh MRS-SM was added and the cells allowed to recover at 30C for 2 hours before plating on MRS + erythromycin +

lincomycin. Colonies were re-selected on identical media and resuspended in MRS + erythromycin + licomycin and grown at 39C overnight. Saturated cultures were diluted 1:100 and plated on MRS + erythromycin + lincomycin and grown at 39C overnight. Colonies were selected and grown in MRS (without antibiotic selection) at 30C for 3 days, with a 1:25 dilution every morning. On the fourth day, cultures were grown at 39C for 8 hours before plating a $1:10^6$ dilution on multiple plates. Colony-containing plates were replica plated onto MRS + erythromycin + liconmycin. Colonies sensitive to antibiotics were selected for colony PCR using primers ~1kB up and downstream of the gene. A PCR product of ~2kB indicated successful loss of YP_296294.

Phenotype verification

Overnight cultures of candidate knockout or knockin strains were prepared alongside the vector controls. In the morning, they diluted into fresh media and allowed to grow at 37C for 90 minutes before being transferred to M9 minimal media containing tryptophan. After 24 hours, cell free supernatant was analyzed by HPLC.

Mouse Experiments

Germ-free (GF) swiss webster mice were maintained in gnotobiotic isolators on a strict 12h light cycle. Four week old GF mice were humanized by oral gavage of 200 µl of human fecal sample prepared by mixing stored frozen human fecal sample obtained from a healthy anonymous donor (male, age 38, American diet) with filter-sterilized pre-reduced phosphate buffered saline and the microbiota was allowed to equilibrate for

additional 4 weeks. Mice were fed autoclaved standard diet (Purina LabDiet 5K67). All animal protocols were in accordance with A-PLAC, the Stanford IACUC. Fresh fecal samples were collected from mice at defined interval and stored at -80C until further processing.

In order to determine the role of bacterial tryptamine on serotonin regulation in the gastrointestinal tract both GF mice (8 wk) and humanized mice (8 wk) were gavaged with 200 µl from an overnight culture in LB medium of either *E. coli* MG1655 + pAH70 (vector control) or *E. coli* MG1655 + RUMGNA_0152. The OD after overnight culture in LB was close to 1 in both strains suggesting similar growth in culture medium. In order to further augment the effect of bacterial tryptamine on host metabolite, the drinking water was sequentially supplemented with 0.25% tryptophan and then 0.25% tryptophan with 0.015% phenelzine (monoamine oxidase inhibitor). Fecal pellets and gastrointestinal transit measurements were done before and after each intervention.

Gastrointestinal transit time

Whole gut transit time was determined using carmine red method as previously described(55). Briefly, to study GI transit time, a dye that cannot be absorbed from the lumen (carmine red) was administered to mice (56). A 6% solution of carmine red (300 µl; Sigma-Aldrich) suspended in 0.5% methylcellulose (Sigma-Aldrich) was administered by gavage through a 21 gauge round-tip feeding needle to non-fasted mice. After gavage, fecal pellets were monitored at 15 min intervals for the presence of red

pellet. Total GI transit time was considered as the interval between *gavage* and the time of first observance of red pellet. .

Colonization confirmation

DNA from representative fecal pellets was prepared using a Zymo ZR Fecal DNA Miniprep kit. A PCR was performed using primers that would amplify RUMGNA_01526.

LC/MS/MS analysis

Fecal pellets were added to 4mL glass vials containing Zymo ZR BeadBashing beads. 0.5mL 50% methanol with 50uM dinitrobenzene was added and vials were sonicated in a water bath for 4 minutes, followed by 15 minutes of vortexing. Using a glass Pasteur pipet, extract was removed and centrifuged for 10 minutes at 15000 rpm. Extract was transferred to a clean centrifuge tube and stored at -20C. 150 μL of extract was loaded into a glass vial for LC/MS/MS analysis.

Chapter 5—Conclusion

The production of tryptamine by *C. sporogenes* was notable for three reasons. First, while the decarboxylation of tryptophan to tryptamine is common in the plant kingdom, tryptophan decarboxylation is an exceedingly rare activity among bacteria(30). To our knowledge, the only bacterial species in which this transformation is known is the entomopathogenic nematode symbiont *Xenorhabdus* and *Bacillus atrophaeus,* which are thought to produce tryptamine as a building block for the biosynthesis of larger natural products (35, 36). *Lactobacillus bulgaricus* is currently the only know bacterial species know to excrete tryptamine (34).

Second, tryptamine is a β-arylamine neurotransmitter known to have a range of biological activities. As a trace amine found in low quantities in the brain, it is a ligand for the trace amine-associated receptors (TAARs) that potentiates the inhibitory response of cells to serotonin, as well as a ligand for the sigma-2 receptor (21, 57, 58). In can inhibit CYP1A2 and the amino acid transporter PAT1 (59, 60). Long forgotten research suggested that tryptamine could indirectly stimulate acetylcholine release, cause vasocontriction, and was found in high levels in the hypothalamus (61-63).

Moreover, tryptamine has been observed in human and rodent feces, where it is known to induce the release of serotonin by enterochromaffin cells (42, 64, 65). Fluctuations in intestinal serotonin levels have several consequences, such as increased GI motility (particularly in the case of cholera (66, 67)), as well as inflammatory bowel diseases (68-70). This activity is especially interesting in light of the critical role serotonin plays as a signaling molecule in the enteric nervous system, where modulation of the serotonin receptors has been proposed as a treatment for irritable bowel syndrome

(71-74). Indeed, the microbiota of IBS patients have been observed to be dominated by the phyla Firmicutes (to which the decarboxylases describe here and those we identified from metagenomic sequencing belong), which raises the question of whether they also have higher levels of tryptophan decarboxylases (75).

Third, tryptamine production represents an intestinal microbiota mediated alteration in tryptophan metabolism. Host serotonin is produced from dietary tryptophan and metabolic profiling has shown that germ-free mice have a 2.8 fold increase in plasma serotonin levels over conventionalized mice (25). Furthermore, Wikoff et al show that germ-free mice have elevated levels of tryptophan. Two additional studies show that germ-free mice have elevated levels of serotonin, 5-HT, and tryptophan without explanatory changes in gene expression of tryptophan utilizing enzymes, and suggest that the microbiota is somehow participating in tryptophan metabolism (76, 77). Our discovery of tryptophan decarboxylases in the human microbiota raises the possibility that microbes can sequester tryptophan from the host and thereby alter brain serotonin levels. We are currently working on a CLOSPO_02083 knockout that will assist in deciphering exactly how tryptophan metabolism into tryptamine is affecting host brain and behavior. Reducing plasma tryptophan would reduce the available substrate for serotonin synthesis in the brain and could represent one way the microbiota influence behavior as the serotonergic signaling system is the major biological substrate in the pathology of mood disorders and anxiety.

Tryptamine has been a relatively understudied neurotransmitter due to the host's inability to synthesize it efficiently and its reduced affinity for 5HT receptors. While the handful of studies summarized above suggest minor roles, the data does not convincingly

demonstrate a unique contribution to the host. However, with this discovery of the microbiota's ability to synthesize tryptamine, there is a dire need to perform in-depth physiology experiments to elucidate its impact on the host both in the intestine and in the brain.

The potential contributions from the human microbiota to host health and physiology are only beginning to be explored. Undoubtedly different organisms will influence every aspect of human health at the molecular level. It will be increasingly important to understand the molecular mechanism behind each interaction. In the work described here, we have identified two resident gut bacteria that are capable of producing tryptamine, a biologically active molecule, and confirmed the genes responsible for production. Tryptamine has the potential to interact with the nervous system, although the physiology of tryptamine in the intestine is currently undefined. Our findings open the door to studying this biogenic amine in finer detail, including characterizing the expression levels of receptors in the gut and how well tryptamine stimulates the neurons in the ENS.

Knowing that the genes exist for tryptamine production in the human gut will serve as a guide to understanding how the micriobiota influence the brain and behavior. The first thing we need to know before understand how relevant this finding is would be to determine the proportion of the human population that harbors these genes. A post-doc in the lab, Mohamed Donia, performed a bioinformatic analysis to evaluate how abundant similar tryptophan decarboxylases were in the human microbiota.

Initial assemblies of sequenced human stool samples from 86 healthy subjects were examined for the presence of similar amino acid decarboxylases. We used BLASTP

to search the metagenomic contigs for homologs of RUMGNA_01526. In total, we identified homologs of RUMGNA_01526 in 15 subjects (17% of the samples). Of those, 13 subjects contained only one decarboxylase homolog, while two subjects harbored two different homologs. Eight subjects (9.3%) contained a tryptophan decarboxylase homolog that is almost identical to the RUMGNA_01526 characterized here (>99% identical at the amino acid level over >100 residues). The rest of the samples harbored decarboxylase homologs that were 62-93% identical to RUMGNA_01526 over >100 residues (Table 5.1). Further biochemical characterization is needed to assign these more distantly related homologs as aromatic amino acid decarboxylases. These homologs were highly similar to genes from a variety of anaerobic Firmicute reference genomes, such as *Clostridium asparagiforme, Clostridium nexile*, *Desulfitobacterium dehalogenans,* and *Blautia hansenii*. Despite the fact that *C. sporogenes* ATCC 15579 is a human gut isolate, similar searches with CLOSPO_02083 yielded no hits. The presence of tryptophan decarboxylase homologs in 9-17% of gut metagenomes of a random population of healthy humans suggests that tryptamine produced by gut bacteria may be more prevalent in humans than previously thought.

Table 5. 1

Accession number of closest homolog	**Source organism of the closest homolog**	**Percent identity to the closest homolog[a]**	**Prevalence in HMP stool samples (N=86 subjects)[b]**
ZP_02040762	*Ruminococcus gnavus*	100%	5 subjects
HMPREF9477_00579	*Lachnospiraceae* bacterium 2_1_58FAA	100%	3 subjects
ZP_05855305	*Blautia hansenii* DSM 20583	99%	1 subject
ZP_02040762 or HMPREF9477_00579	*Ruminococcus gnavus* or *Lachnospiraceae* bacterium 2_1_58FAA	93%	1 subject
WP_004612385	*Clostridium nexile*	77%	1 subject
YP_006429963	*Desulfitobacterium dehalogenans* ATCC 51507	67%	2 subjects
WP_007718072	*Clostridium asparagiforme*	62%	4 subjects

Table 5.1 Presence of tryptophan decarboxylases in the Human Microbiome Project Samples

[a]BLAST percent identity was calculated for at least 100 amino acids

[b]15 subjects were found to contain homologs of the putative tryptophan decarboxylases. Of those, two contained two different homologs, and 13 contained one homolog.

(Analysis performed by Mohamed Donia)

The next question will be to understand how tryptamine is regulating human physiology. We know that serotonin is produced in large quantities in the gut and plays several roles, most notably regulating GI motility (78). It has also been shown that tryptamine can induce serotonin release in the gut, although at high concentrations (1-3 mM) (42). However, despite this knowledge, the physiological response to intestinal tryptamine has not been elucidated. Initial characterization of tryptamine levels in germ-free and conventional mice would determine the extent to which microbiota contribute to the pool of available tryptamine. Our initial studies in mice colonized with only *E. coli* MG1655 suggest that mice without bacteria containing a tryptophan decarboxylase do not contain tryptamine. Going forward, it will be interesting to quantify the amount of tryptamine produced by the microbiota, as well as comparing the intestinal physiology of mice colonized with a wild type and decarboxylase-knockout strain of bacteria. Additionally, extensive studies into tryptamine's affinity for serotonin receptors would elucidate the potential activity of bacterial-produced tryptamine. Tryptamine is also known to stimulate the trace amine receptor (TAAR), but the levels of this receptor in the gut are currently unknown.

One of the most interesting lines of investigation that our work reveals is studying how bacterially produced tryptamine affects the brain and behavior. To this end, it would be exciting to generate a knockout strain of *Ruminococcus gnavus* that is unable to produce tryptamine and perform behavioral comparisons between germ-free mice that have either the wild-type or knock-out strain such as the open field test, Sudo and Hsiao (18, 20). Similar to the study performed by Bravo et al, it would be very interesting to

sever the vagus nerve to confirm the connection between the gut and effects on the brain (19).

An additional experiment that would help us to confirm the idea that bacterially produced molecules are capable of influencing the brain would be to use the decarboxylase we found in *Ruminococcus gnavus* to make a molecule that clearly influences behavior. Tryptamine is the precursor to several molecules, one of which is the psychoactive compound dimethyltryptamine (DMT). This molecule is currently a street drug with known hallucinogenic effects. The chemical transformation from tryptamine into DMT is possible through a single enzyme, an indole-N-methyltransferase (INMT) (58). The human genome contains an INMT that is used to methylate tryptamine and structurally related molecules (79, 80). By engineering a strain of bacteria that is capable of producing DMT through the coexpression of a tryptophan decarboxylase and an INMT, we would essentially create a platform to study the molecular connection between the gut and the brain. Do molecules produced in the gut travel through the blood stream and cross the blood brain barrier? Or perhaps do they stimulate neuronal neurons through the ENS? Although an entirely artificial system, colonization of germ-free mice with this new strain of bacteria would be one powerful way to study the effect of bacterially produced molecules on behavior.

Our understanding of how gut microbes interact with the nervous system is in its infancy. It will require a concerted effort between chemistry, molecular biology, genetics, and neuroscience to fully elucidate the extensive communication network between the gut and the brain. However, as we gain understanding, we acquire access to a new target for treating patients suffering from diseases that are influenced by the microbiota.

References

1. Zhu B, Wang X, Li L (2010) Human gut microbiome: the second genome of human body. *Protein Cell* 1:718–725.

2. Turnbaugh PJ et al. (2006) An obesity-associated gut microbiome with increased capacity for energy harvest. *Nature* 444:1027–131.

3. Qin J et al. (2012) A metagenome-wide association study of gut microbiota in type 2 diabetes. *Nature* 490:55–60.

4. Sartor RB (2008) Microbial influences in inflammatory bowel diseases. *Gastroenterology* 134:577–594.

5. Nell S, Suerbaum S, Josenhans C (2010) The impact of the microbiota on the pathogenesis of IBD: lessons from mouse infection models. *Nat Rev Microbiol* 8:564–577.

6. Macfarlane S, Macfarlane GT (2007) Regulation of short-chain fatty acid production. *Proc Nutr Soc* 62:67–72.

7. Xiong Y et al. (2004) Short-chain fatty acids stimulate leptin production in adipocytes through the G protein-coupled receptor GPR41. *Science Signaling* 101:1045.

8. Tolhurst G et al. (2012) Short-Chain Fatty Acids Stimulate Glucagon-Like Peptide-1 Secretion via the G-Protein-Coupled Receptor FFAR2. *Diabetes* 61:364–371.

9. Peterson DA, McNulty NP, Guruge JL, Gordon JI (2007) IgA response to symbiotic bacteria as a mediator of gut homeostasis. *Cell Host Microbe* 2:328–339.

10. Chung H et al. (2012) Gut immune maturation depends on colonization with a host-specific microbiota. *Cell* 149:1578–1593.

11. Hill DA, Artis D (2010) Intestinal bacteria and the regulation of immune cell homeostasis. *Annu Rev Immunol* 28:623–667.

12. Backhed F, Ley R, Sonnenburg J, Peterson D, Gordon J (2005) Host-bacterial mutualism in the human intestine. *Science* 307:1915–1920.

13. Mazmanian SK, Liu CH, Tzianabos AO, Kasper DL (2005) An Immunomodulatory Molecule of Symbiotic Bacteria Directs Maturation of the Host Immune System. *Cell* 122:107–118.

14. Round JL et al. (2011) The Toll-Like Receptor 2 Pathway Establishes Colonization by a Commensal of the Human Microbiota. *Science* 332:974–977.

15. Koeth RA et al. (2013) Intestinal microbiota metabolism of L-carnitine, a nutrient in red meat, promotes atherosclerosis. *Nat Med*:1–12.

16. Goyal RK, Hirano I (1996) The enteric nervous system. *N Engl J Med* 334:1106–1115.

17. Gershon MD (1981) The enteric nervous system. *Annu Rev Neurosci* 4:227–272.

18. Sudo N et al. Postnatal microbial colonization programs the hypothalamic–pituitary–adrenal system for stress response in mice. *jpphysocorg*.

19. Bravo JA et al. (2011) Ingestion of Lactobacillus strain regulates emotional behavior and central GABA receptor expression in a mouse via the vagus nerve. *P Natl Acad Sci Usa* 108:16050–16055.

20. Hsiao EY et al. (2013) Microbiota Modulate Behavioral and Physiological Abnormalities Associated with Neurodevelopmental Disorders. *Cell* 155:1451–1463.

21. Zucchi R, Chiellini G, Scanlan TS, Grandy DK (2006) Trace amine-associated receptors and their ligands. *Brit J Pharmacol* 149:967–978.

22. Moreno-Arribas V, Lonvaud-Funel A (2001) Purification and characterization of tyrosine decarboxylase of Lactobacillus brevis IOEB 9809 isolated from wine. *FEMS Microbiol Lett* 195:103–107.

23. Marcobal A, las Rivas de B, Muñoz R (2006) First genetic characterization of a bacterial beta-phenylethylamine biosynthetic enzyme in Enterococcus faecium RM58. *FEMS Microbiol Lett* 258:144–149.

24. Gable RS (2007) Risk assessment of ritual use of oral dimethyltryptamine (DMT) and harmala alkaloids. *Addiction* 102:24–34.

25. Wikoff WR et al. (2009) Metabolomics analysis reveals large effects of gut microflora on mammalian blood metabolites. *P Natl Acad Sci Usa* 106:3698–3703.

26. John RA (1995) Pyridoxal phosphate-dependent enzymes. *Biochim Biophys Acta* 1248:81–96.

27. Schneider G, Käck H, Lindqvist Y (2000) The manifold of vitamin B6 dependent enzymes. *Structure*.

28. GALLAGHER T, ROZWARSKI D, ERNST S, HACKERT M (1993) REFINED STRUCTURE OF THE PYRUVOYL-DEPENDENT HISTIDINE-DECARBOXYLASE FROM LACTOBACILLUS-30A. *J Mol Biol* 230:516–528.

29. BLACKWELL B, MARLEY E (1964) INTERACTION BETWEEN CHEESE AND MONOAMINE-OXIDASE INHIBITORS IN RATS AND CATS. *Lancet* 1:530–531.

30. Facchini PJ, Huber-Allanach KL, Tari LW (2000) Plant aromatic L-amino acid decarboxylases: evolution, biochemistry, regulation, and metabolic engineering applications. *Phytochemistry* 54:121–138.

31. Ishihara A et al. (2011) Probing the role of tryptophan-derived secondary metabolism in defense responses against Bipolaris oryzae infection in rice leaves by a suicide substrate of tryptophan decarboxylase. *Phytochemistry* 72:7–13.

32. Mano Y, Nemoto K (2012) The pathway of auxin biosynthesis in plants. *Journal of Experimental Botany* 63:2853–2872.

33. El-Sayed M, Verpoorte R (2007) Catharanthus terpenoid indole alkaloids: biosynthesis and regulation. *Phytochem Rev* 6:277–305.

34. CHANDER H, Batish VK, Babu S, Singh RS (1989) Factors affecting amine production by a selected strain of Lactobacillus bulgaricus. *Journal of Food Science* 54:940–942.

35. Proschak A et al. (2011) Cytotoxic fatty acid amides from Xenorhabdus. *Chembiochem* 12:2011–2015.

36. Yuwen L et al. (2013) The role of aromatic L-amino acid decarboxylase in bacillamide C biosynthesis by Bacillus atrophaeus C89. *Sci Rep* 3.

37. Toney MD (2005) Reaction specificity in pyridoxal phosphate enzymes. *Archives of Biochemistry and Biophysics* 433:279–287.

38. Eliot AC, Kirsch JF (2004) Pyridoxal phosphate enzymes: mechanistic, structural, and evolutionary considerations. *Annu Rev Biochem* 73:383–415.

39. Mozzarelli A, Bettati S (2006) Exploring the pyridoxal 5'-phosphate-dependent enzymes. *Chem Rec* 6:275–287.

40. Fenalti G et al. (2007) GABA production by glutamic acid decarboxylase is regulated by a dynamic catalytic loop. *Nat Struct Mol Biol* 14:280–286.

41. Bianchetti MG, Minder I, Beretta-Piccoli C, Meier A (1982) Effects of tyramine on blood pressure and plasma catecholamines in normal and hypertensive subjects. *Klinische ...*.

42. Takaki M, Mawe GM, Barasch JM, Gershon MD, Gershon MD (1985) Physiological responses of guinea-pig myenteric neurons secondary to the release of endogenous serotonin by tryptamine. *Neuroscience* 16:223–240.

43. BHATTACHARJEE MK, Snell EE (1990) Pyridoxal 5'-Phosphate-Dependent Histidine-Decarboxylase - Mechanism of Inactivation by Alpha-Fluoromethylhistidine. *J Biol Chem* 265:6664–6668.

44. Hayashi H, Tanase S, Snell EE (1986) Pyridoxal 5'-phosphate-dependent histidine decarboxylase. Inactivation by alpha-fluoromethylhistidine and comparative sequences at the inhibitor- and coenzyme-binding sites. *J Biol Chem* 261:11003–11009.

45. Giardina G, Montioli R, Gianni S (2011).

46. Burkhard P, Dominici P, Borri Voltattorni C, Jansonius JN, Malashkevich VN (2001) Structural insight into Parkinson's disease treatment from drug-inhibited DOPA decarboxylase. *Nat Struct Biol* 8:963–967.

47. Schirmer A, Kennedy J, Murli S, Reid R, Santi DV (2006) Targeted covalent inactivation of protein kinases by resorcylic acid lactone polyketides. *P Natl Acad Sci Usa* 103:4234–4239.

48. Kuehne SA, Minton NP (2012) ClosTron-mediated engineering of Clostridium. *Bioengineered* 3:247–254.

49. Sikander A, Rana SV, Prasad KK (2009) Role of serotonin in gastrointestinal motility and irritable bowel syndrome. *Clin Chim Acta* 403:47–55.

50. Karberg M et al. (2001) Group II introns as controllable gene targeting vectors for genetic manipulation of bacteria. *Nat Biotechnol* 19:1162–1167.

51. Pritzlaff CA et al. (2001) Genetic basis for the beta-haemolytic/cytolytic activity of group B Streptococcus. *Mol Microbiol* 39:236–248.

52. Blancato V, Magni C (2010) A chimeric vector for efficient chromosomal modification in Enterococcus faecalisand other lactic acid bacteria. *Letters in Applied Microbiology* 50:542–546.

53. Haldimann A, Wanner BL (2001) Conditional-replication, integration, excision, and retrieval plasmid-host systems for gene structure-function studies of bacteria. *J Bacteriol* 183:6384–6393.

54. Gershon MD (2005) Nerves, reflexes, and the enteric nervous system: pathogenesis of the irritable bowel syndrome. *J Clin Gastroenterol* 39:S184–93.

55. Li Z et al. (2011) Essential roles of enteric neuronal serotonin in gastrointestinal motility and the development/survival of enteric dopaminergic neurons. *J Neurosci* 31:8998–9009.

56. Kimball ES, Palmer JM, D'Andrea MR, Hornby PJ, Wade PR (2005) Acute colitis induction by oil of mustard results in later development of IBS-like accelerated

upper GI transit in mice. *Am J Physiol-Gastr L* 288:G1266–G1273.

57. Borowsky B et al. (2001) Trace amines: identification of a family of mammalian G protein-coupled receptors. *P Natl Acad Sci Usa* 98:8966–8971.

58. Fontanilla D et al. (2009) The hallucinogen N,N-dimethyltryptamine (DMT) is an endogenous sigma-1 receptor regulator. *Science* 323:934–937.

59. Agundez J, Gallardo L, Martinez C, Gervasini G, Benitez J (1998) Modulation of CYP1A2 enzyme activity by indoleamines: inhibition by serotonin and tryptamine. *Pharmacogenetics* 8:251–258.

60. Metzner L, Kottra G, Neubert K, Daniel H, Brandsch M (2005) Serotonin, L-tryptophan, and tryptamine are effective inhibitors of the amino acid transport system PAT1. *FASEB J* 19:1468–1473.

61. Ennis C, Cox B (1982) The effect of tryptamine on serotonin release from hypothalamic slices is mediated by a cholinergic interneurone. *Psychopharmacology (Berl)* 78:85–88.

62. Anwar MA, Ford WR, Broadley KJ (2012) Vasoconstrictor and vasodilator responses to tryptamine of rat‐isolated perfused mesentery: comparison with tyramine and β‐phenylethylamine. *British journal of …*.

63. Knott PJ, Marsden CA, Curzon G (1974) Comparative studies of brain 5-hydroxytryptamine and tryptamine. *Adv Biochem Psychopharmacol* 11:109–114.

64. ANDERSON G (1975) QUANTITATION OF TRYPTOPHAN-METABOLITES IN RAT FECES BY THIN-LAYER CHROMATOGRAPHY. *J Chromatogr* 105:323–328.

65. Brooks JB, Nunez-Montiel OL, Basta MT, Hierholzer JC (1984) Studies of stools from pseudomembranous colitis, rotaviral, and other diarrheal syndromes by frequency-pulsed electron capture gas-liquid chromatography. *J Clin Microbiol* 20:549–560.

66. Lundgren O (1998) 5-Hydroxytryptamine, enterotoxins, and intestinal fluid secretion. *Gastroenterology* 115:1009–1012.

67. Turvill JL, Connor P, Farthing MJ (2000) The inhibition of cholera toxin-induced 5-HT release by the 5-HT(3) receptor antagonist, granisetron, in the rat. *Brit J Pharmacol* 130:1031–1036.

68. Linden DR et al. (2005) Serotonin transporter function and expression are reduced in mice with TNBS-induced colitis. *Neurogastroenterol Motil* 17:565–574.

69. Linden DR, Chen J-X, Gershon MD, Sharkey KA, Mawe GM (2003) Serotonin availability is increased in mucosa of guinea pigs with TNBS-induced colitis. *Am J*

Physiol-Gastr L 285:G207–16.

70. Bischoff SC et al. (2009) Role of serotonin in intestinal inflammation: knockout of serotonin reuptake transporter exacerbates 2,4,6-trinitrobenzene sulfonic acid colitis in mice. *Am J Physiol-Gastr L* 296:G685–95.

71. Mayer EA (2011) Gut feelings: the emerging biology of gut-brain communication. *Nat Rev Neurosci* 12:453–466.

72. Gershon MD, Tack J (2007) The Serotonin Signaling System: From Basic Understanding To Drug Development for Functional GI Disorders. *Gastroenterology*.

73. Ormsbee HS, Fondacaro JD (1985) Action of serotonin on the gastrointestinal tract. *Proc Soc Exp Biol Med* 178:333–338.

74. Mawe GM, Coates MD, Moses PL (2006) Review article: intestinal serotonin signalling in irritable bowel syndrome. *Aliment Pharmacol Ther* 23:1067–1076.

75. Jeffery IB et al. (2012) An irritable bowel syndrome subtype defined by species-specific alterations in faecal microbiota. *Gut* 61:997–1006.

76. Clarke G et al. (2012) The microbiome-gut-brain axis during early life regulates the hippocampal serotonergic system in a sex-dependent manner. *Mol Psychiatr* 18:666–673.

77. Heijtz RD et al. Normal gut microbiota modulates brain development and behavior. *pnasorg*.

78. Bertrand PP, Bertrand RL (2010) Serotonin release and uptake in the gastrointestinal tract. *Auton Neurosci-Basic* 153:47–57.

79. Thompson MA et al. (1999) Human indolethylamine N-methyltransferase: cDNA cloning and expression, gene cloning, and chromosomal localization. *Genomics* 61:285–297.

80. MANDELL AJ, MORGAN M (1971) Indole(ethyl)amine N-Methyltransferase in Human Brain. *Nat New Biol* 230:85–87.

Appendix A: Table of bacterial growth conditions

Strain	Atmosphere	Temperature	Media
E. coli Tg1	Aerobic	37	LB
E. coli BL21 (DE3)	Aerobic	37	LB
Bifidobacterium dentium	Anaerobic	37	RCM
Clostridium sporogenes	Anaerobic	37	RCM
Parabacteroides distasonis	Anaerobic	37	RCM
Bacteroides vulgatus	Anaerobic	37	Bacteroides rich medium
Bacteroides fragilis	Anaerobic	37	Bacteroides rich medium
Pseudomonas putida	Aerobic	30	Nutrient Broth
Lactobacillus brevis	Aerobic	30	MRS
Lactobacillus oris	Anaerobic	30	MRS
Photorhabdus luminescens	Aerobic	30	Nutrient Broth
Providencia stuartii	Aerobic	37	Nutrient Broth
Staphylococcus epidermis	Aerobic	37	TSB
Ruminococcus gnavus	Anaerobic	37	RCM
Lactobacillus vaginalis	Aerobic	30	MRS
Enterococcus faecalis	Aerobic	37	BHI

Appendix B: Table of Primers

ID number	Description	Sequence
BBW2-1	E. coli BL21 ZP_00712862, pET24b forward	AGAAGGAGATATACATATGGCTAGCATGGATAAGAAGCAAGTA
BBW2-2	E. coli BL21 ZP_00712862, pET24b reverse	AGTGGTGGTGGTGGTGGTGCTCGAGTTCAGGTATGTTTAAAGCT
BBW2-3	E. coli BL21 ZP_00712862, pET28a forward	CCTGGTGCCGCGCGGCAGCCATATGATGGATAAGAAGCAAGTA
BBW2-4	E. coli BL21 ZP_00712862, pET28a reverse	GTGGTGGTGGTGGTGGTGCTCGAGTTCAGGTATGTTTAAAGCT
BBW2-5	E. coli BL21 ACT45166, pET24b forward	AGAAGGAGATATACATATGGCTAGCATGGACCAGAAGCTGTTA
BBW2-6	E. coli BL21 ACT45166, pET24b reverse	AGTGGTGGTGGTGGTGGTGCTCGAGTTCAGGTGTGTTTAAAGCT
BBW2-7	E. coli BL21 ACT45166, pET28a forward	CCTGGTGCCGCGCGGCAGCCATATGATGGACCAGAAGCTGTTA
BBW2-8	E. coli BL21 ACT45166, pET28a reverse	GTGGTGGTGGTGGTGGTGCTCGAGTTCAGGTGTGTTTAAAGCT
BBW2-9	Bifidobacterium dentium ZP_02918104, pET24b forward	AGAAGGAGATATACATATGGCTAGCATGTCGATAATGCATTCC
BBW2-10	Bifidobacterium dentium ZP_02918104, pET24b reverse	AGTGGTGGTGGTGGTGGTGCTCGAGTTCAGTGATGGAAGCCGGA
BBW2-11	Bifidobacterium dentium ZP_02918104, pET28a forward	CCTGGTGCCGCGCGGCAGCCATATGATGTCGATAATGCATTCC
BBW2-12	Bifidobacterium dentium ZP_02918104, pET28a reverse	GTGGTGGTGGTGGTGGTGCTCGAGTTCAGTGATGGAAGCCGGA
BBW2-13	Parabacteroides distasonis YP_001302213, pET24b forward	AGAAGGAGATATACATATGGCTAGCATGAAAGACTCAAATTTC
BBW2-14	Parabacteroides distasonis YP_001302213, pET24b reverse	AGTGGTGGTGGTGGTGGTGCTCGAGTTTATTTCTTAGCGTTGCT
BBW2-15	Parabacteroides distasonis YP_001302213, pET28a forward	CCTGGTGCCGCGCGGCAGCCATATGATGAAAGACTCAAATTTC
BBW2-16	Parabacteroides distasonis YP_001302213, pET28a reverse	GTGGTGGTGGTGGTGGTGCTCGAGTTTATTTCTTAGCGTTGCT
BBW2-17	Bacteroides vulgatus	AGAAGGAGATATACATATGGCTAGCATGAAAGAATGTAATTGT

	YP_001301120, pET24b forward	
BBW2-18	Bacteroides vulgatus YP_001301120, pET24b reverse	AGTGGTGGTGGTGGTGGTGCTCGAGTTTATTTTTTAGCGGCGTT
BBW2-19	Bacteroides vulgatus YP_001301120, pET28a forward	CCTGGTGCCGCGCGGCAGCCATATGATGAAAGAATGTAATTGT
BBW2-20	Bacteroides vulgatus YP_001301120, pET28a reverse	GTGGTGGTGGTGGTGGTGCTCGAGTTTATTTTTTAGCGGCGTT
BBW2-21	Bacteroides fragilis YP_21022, pET24b forward	AGAAGGAGATATACATATGGCTAGCATGGAAGATTTAAATTTC
BBW2-22	Bacteroides fragilis YP_21022, pET24b reverse	AGTGGTGGTGGTGGTGGTGCTCGAGTTTATTTCTTGGCAGCTTG
BBW2-23	Bacteroides fragilis YP_21022, pET28a forward	CCTGGTGCCGCGCGGCAGCCATATGATGGAAGATTTAAATTTC
BBW2-24	Bacteroides fragilis YP_21022, pET28a reverse	GTGGTGGTGGTGGTGGTGCTCGAGTTTATTTCTTGGCAGCTTG
BBW2-25	Photorhabdus luminescens NP_929587, pET24b forward	AGAAGGAGATATACATATGGCTAGCATGATTATGACCAAGCAG
BBW2-26	Photorhabdus luminescens NP_929587, pET24b reverse	AGTGGTGGTGGTGGTGGTGCTCGAGTTCAGGCCACTTTCTTTTT
BBW2-27	Photorhabdus luminescens NP_929587, pET28a forward	CCTGGTGCCGCGCGGCAGCCATATGATGATTATGACCAAGCAG
BBW2-28	Photorhabdus luminescens NP_929587, pET28a reverse	GTGGTGGTGGTGGTGGTGCTCGAGTTCAGGCCACTTTCTTTTT
BBW2-29	Pseudomonas entomophilia YP_607981, pET24b forward	AGAAGGAGATATACATATGGCTAGATGACCCCCGAACAATTC
BBW2-30	Pseudomonas entomophilia YP_607981, pET24b reverse	AGTGGTGGTGGTGGTGGTGCTCGAGTTCAGGCCACGACGGTTTG
BBW2-31	Pseudomonas entomophilia YP_607981, pET28a forward	CCTGGTGCCGCGCGGCAGCCATATGATGACCCCCGAACAATTC
BBW2-32	Pseudomonas entomophilia YP_607981, pET28a reverse	GTGGTGGTGGTGGTGGTGCTCGAGTTCAGGCCACGACGGTTTG
BBW2-33	Pseudomonas putida NP_744697, pET24b forward	AGAAGGAGATATACATATGGCTAGCATGACCCCCGAACAATTC
BBW2-34	Pseudomonas putida NP_744697, pET24b reverse	AGTGGTGGTGGTGGTGGTGCTCGAGTTCAGCCCTTGATCACGTC

BBW2-35	Pseudomonas putida NP_744697, pET28a forward	CCTGGTGCCGCGCGGCAGCCATATGATGACCCCCGAACAATTC
BBW2-36	Pseudomonas putida NP_744697, pET28a reverse	GTGGTGGTGGTGGTGGTGCTCGAGTTCAGCCCTTGATCACGTC
BBW2-37	Lactobacillus oris ZP_07729457, pET24b forward	AGAAGGAGATATACATATGGCTAGCATGACTGAAAAAAGCCGC
BBW2-38	Lactobacillus oris ZP_07729457, pET24b reverse	AGTGGTGGTGGTGGTGGTGCTCGAGTTTAACCTAAGATAGCGGT
BBW2-39	Lactobacillus oris ZP_07729457, pET28a forward	CCTGGTGCCGCGCGGCAGCCATATGATGACTGAAAAAAGCCGC
BBW2-40	Lactobacillus oris ZP_07729457, pET28a reverse	GTGGTGGTGGTGGTGGTGCTCGAGTTTAACCTAAGATAGCGGT
BBW2-41	Providencia stuartii ZP_02960556, pET24b forward	AGAAGGAGATATACATATGGCTAGCATGACAAATTTTAATAAC
BBW2-42	Providencia stuartii ZP_02960556, pET24b reverse	AGTGGTGGTGGTGGTGGTGCTCGAGTTTATAGCGTTATTTTTTG
BBW2-43	Providencia stuartii ZP_02960556, pET28a forward	CCTGGTGCCGCGCGGCAGCCATATGATGACAAATTTTAATAAC
BBW2-44	Providencia stuartii ZP_02960556, pET28a reverse	GTGGTGGTGGTGGTGGTGCTCGAGTTTATAGCGTTATTTTTTG
BBW2-45	Enterococcus faecalis NP_814388, pET24b forward	AGAAGGAGATATACATATGGCTAGCATGAATGCAAAATCTAAT
BBW2-46	Enterococcus faecalis NP_814388, pET24b reverse	AGTGGTGGTGGTGGTGGTGCTCGAGTTTATTTTACGTCGTAAAT
BBW2-47	Enterococcus faecalis NP_814388, pET28a forward	CCTGGTGCCGCGCGGCAGCCATATGATGAATGCAAAATCTAAT
BBW2-48	Enterococcus faecalis NP_814388, pET28a reverse	GTGGTGGTGGTGGTGGTGCTCGAGTTTATTTTACGTCGTAAAT
BBW2-49	Dickey zeae YP_003002643, pET24b forward	AGAAGGAGATATACATATGGCTAGCATGCAACCGGTTGATGAG
BBW2-50	Dickey zeae YP_003002643, pET24b reverse	AGTGGTGGTGGTGGTGGTGCTCGAGTTCACGCCTCCTTCTCTGT
BBW2-51	Dickey zeae YP_003002643, pET28a forward	CCTGGTGCCGCGCGGCAGCCATATGATGCAACCGGTTGATGAG
BBW2-52	Dickey zeae YP_003002643, pET28a reverse	GTGGTGGTGGTGGTGGTGCTCGAGTTCACGCCTCCTTCTCTGT
BBW2-53	Staphylococcus epidermis NP_763667, pET24b forward	AGAAGGAGATATACATATGGCTAGCATGGAAATGGAATTCAAT
BBW2-54	Staphylococcus epidermis NP_763667,	AGTGGTGGTGGTGGTGGTGCTCGAGTTTAAGCATCTTTCATATC

	pET24b reverse	
BBW2-55	Staphylococcus epidermis NP_763667, pET28a forward	CCTGGTGCCGCGCGGCAGCCATATGATGGAAATGGAATTCAAT
BBW2-56	Staphylococcus epidermis NP_763667, pET28a reverse	GTGGTGGTGGTGGTGGTGCTCGAGTTTAAGCATCTTTCATATC
BBW2-57	Ruminococcus gnavus ZP_02040762, pET24b forward	AGAAGGAGATATACATATGGCTAGCATGAGTCAAGTAATTAAG
BBW2-58	Ruminococcus gnavus ZP_02040762, pET24b reverse	AGTGGTGGTGGTGGTGGTGCTCGAGTTTAAGCTTTTTTCATTTC
BBW2-59	Ruminococcus gnavus ZP_02040762, pET28a forward	CCTGGTGCCGCGCGGCAGCCATATGATGAGTCAAGTAATTAAG
BBW2-60	Ruminococcus gnavus ZP_02040762, pET28a reverse	GTGGTGGTGGTGGTGGTGCTCGAGTTTAAGCTTTTTTCATTTC
BBW2-61	Staphylococcus carnosus YP_002635534, pET24b forward	AGAAGGAGATATACATATGGCTAGCATGGAATTTAACGAAAAC
BBW2-62	Staphylococcus carnosus YP_002635534, pET24b reverse	AGTGGTGGTGGTGGTGGTGCTCGAGTTTAAGCATCTTTCATTTC
BBW2-63	Staphylococcus carnosus YP_002635534, pET28a forward	CCTGGTGCCGCGCGGCAGCCATATGATGGAATTTAACGAAAAC
BBW2-64	Staphylococcus carnosus YP_002635534, pET28a reverse	GTGGTGGTGGTGGTGGTGCTCGAGTTTAAGCATCTTTCATTTC
BBW2-65	Lactobacillus brevis YP_79541, pET28a forward	CCTGGTGCCGCGCGGCAGCCATATGATGGCTATGTTGTATGGA
BBW2-66	Lactobacillus brevis YP_79541, pET28a reverse	GTGGTGGTGGTGGTGGTGCTCGAGTTTAGTGCGTGAACCCGTA
BBW2-67	Lactobacillus brevis YP_794284, pET24b forward	AGAAGGAGATATACATATGGCTAGCATGAATAAAAACGATCAG
BBW2-68	Lactobacillus brevis YP_794284, pET24b reverse	AGTGGTGGTGGTGGTGGTGCTCGAGTTTAACTTCGAACGGTGGT
BBW2-69	Lactobacillus brevis YP_794284, pET28a forward	CCTGGTGCCGCGCGGCAGCCATATGATGAATAAAAACGATCAG
BBW2-70	Lactobacillus brevis YP_794284, pET28a reverse	GTGGTGGTGGTGGTGGTGCTCGAGTTTAACTTCGAACGGTGGT
BBW2-71	Lactobacillus brevis 1kB upstream, pMAD forward	AATCTAGCTAATGTT ACGTTACACATTAACTAGACAGATCT CAAGCAGATAATTGAATC

BBW2-72	Lactobacillus brevis 1kB upstream, reverse (to assemble with 1kB downstream)	AATCTGCAGGAGGTAAGTGACATGG TTAAGCCAATCAATCCAG
BBW2-73	Lactobacillus brevis 1kB downstream, forward (to assemble with 1kB upstream)	AGTCAAACTGGATTGATTGGCTTAA CCATGTCACTTACCTCCT
BBW2-74	Lactobacillus brevis 1kB downstream, pMAD reverse	CCATATGACGTCGAC GCGTCTGCAGAAGCTTCTAGAATTC ATACTGGCATTTCATTTA
BBW2-75	Eggerthella lenta YP_003182843, pET24b forward	AGAAGGAGATATACATATGGCTAGCATGAAGAACGTTGAGGAG
BBW2-76	Eggerthella lenta YP_003182843, pET24b reverse	AGTGGTGGTGGTGGTGGTGCTCGAGTTTACGCGATGTCCGTGAG
BBW2-77	Eggerthella lenta YP_003182843, pET28a forward	CCTGGTGCCGCGCGGCAGCCATATGATGAAGAACGTTGAGGAG
BBW2-78	Eggerthella lenta YP_003182843, pET28a reverse	GTGGTGGTGGTGGTGGTGCTCGAGTTTACGCGATGTCCGTGAG
BBW2-79	Lactobacillus vaginalis ZP_03960099, pET24b forward	AGAAGGAGATATACATATGGCTAGCATGTCCGAATTAGATACG
BBW2-80	Lactobacillus vaginalis ZP_03960099, pET24b reverse	AGTGGTGGTGGTGGTGGTGCTCGAGTTTAGTATTTAACAGCGCC
BBW2-81	Lactobacillus vaginalis ZP_03960099, pET28a forward	CCTGGTGCCGCGCGGCAGCCATATGATGTCCGAATTAGATACG
BBW3-1	Lactobacillus vaginalis ZP_03960099, pET28a reverse	GTGGTGGTGGTGGTGGTGCTCGAGTTTAGTATTTAACAGCGCC
BBW3-4	Bacteroides fragilis YP_211074, pET24b forward	AGAAGGAGATATACATATGGCTAGCATGAAAGATCTTGTGTCC
BBW3-5	Bacteroides fragilis YP_211074, pET24b reverse	AGTGGTGGTGGTGGTGGTGCTCGAGTCTATTCGAAGATCGTCAA
BBW3-6	Bacteroides vulgatus YP_001297671, pET24b forward	AGAAGGAGATATACATATGGCTAGCATGAAAGAATTAGAATTA
BBW3-7	Bacteroides vulgatus YP_001297671, pET24b reverse	AGTGGTGGTGGTGGTGGTGCTCGAGTTTATCCTTCTTTGACTTT
BBW3-8	Ruminococcus gnavus ZP_02040762, pKM079 forward	AAATCGCCATTCGCCAGGGGGATCCCGGAAAAAGGACGCCCGG
BBW3-9	Ruminococcus gnavus ZP_02040762, pKM079 reverse	CCTCTAGATAGCGCATGCTGAATTCAGACGATCTCCCAGTCTT

BBW3-10	Ruminococcus gnavus ZP_02040762, pKM082 forward	GAGGGTTGCCAGAGTTAAAGGATCCCGGAAAAAGGACGCCCGG
BBW3-11	Ruminococcus gnavus ZP_02040762, pKM082 reverse	CCTCTAGATAGCGCATGCTGAATTCAGACGATCTCCCAGTCTT
BBW3-12	Clostridium sporogenes ZP_02994961, pKM079 forward	AAATCGCCATTCGCCAGGGGGATCCGGAATACCAGGAACTAAA
BBW3-13	Clostridium sporogenes ZP_02994961, pKM079 reverse	CCTCTAGATAGCGCATGCTGAATTCTCTATAGTTACTATGTTC
BBW3-14	Clostridium sporogenes ZP_02994961, pKM082 forward	GAGGGTTGCCAGAGTTAAAGGATCCGGAATACCAGGAACTAAA
BBW3-15	Clostridium sporogenes ZP_02994961, pKM082 reverse	CCTCTAGATAGCGCATGCTGAATTCTCTATAGTTACTATGTTC
BBW3-16	pTrc, pAH70 forward	CTGCAGCTGTCCGGAACTAGTCTCGAGTTGACAATTAA
BBW3-17	lac5, pAH70 forward	CTGCAGCTGTCCGGAACTAGTGTCTTCACCTCGAGAAA
BBW3-18	pTrc/Ruminococcus gnavus (for pTrc amplification)	CTTAATTACTTGACTCATATGTATATCTCCTTCTTA
BBW3-19	lac5/Ruminococcus gnavus (for lac5 amplification)	CTTAATTACTTGACTCATATGTATATCTCCTTCTTA
BBW3-20	pTrc/Ruminococcus gnavus (for R. gnavus amplification)	TAAGAAGGAGATATACATATGAGTCAAGTAATTAAG
BBW3-21	lac5/Ruminococcus gnavus (for R. gnavus amplification)	TAAGAAGGAGATATACATATGAGTCAAGTAATTAAG
BBW3-22	Ruminococcus gnavus ZP_02040762, pAH70	ATTCGAGCTCGGTACCCGGGGATCCTTAAGCTTTTTTCATTTC
BBW3-23	Ruminococcus gnavus ZP_02040762, pAH70	GTACCTCTAGACAGGAGACCATATGATGAGTCAAGTAATTAAG
BBW3-24	Ruminococcus gnavus ZP_02040762, pHY304 forward	ATTGGGTACCGGGCCCCCCCTCGAGCGGAAAAAGGACGCCCGG
BBW3-25	Ruminococcus gnavus ZP_02040762, pHY304 reverse	CCACCGCGGTGGCGGCCGCTCTAGAAGACGATCTCCCAGTCTT
BBW3-26	Clostridium sporogenes ZP_02994961, pHY304 forward	ATTGGGTACCGGGCCCCCCCTCGAGGGAATACCAGGAACTAAA
BBW3-27	Clostridium sporogenes ZP_02994961,	CCACCGCGGTGGCGGCCGCTCTAGATCTATAGTTACTATGTTC

	pHY304 reverse	
BBW3-28	Ruminococcus gnavus ZP_02040762, pHY304 forward	GACGGTATCGATAAGCTTCATCAGGAGGACAAAATC
BBW3-29	Ruminococcus gnavus ZP_02040762, pHY304 reverse	TCTAGAACTAGTGGATCCAGACGATCTCCCAGTCTT
BBW3-30	Clostridium sporogenes ZP_02994961, pHY304 forward	GACGGTATCGATAAGCTTGGAATACCAGGAACTAAA
BBW3-31	Clostridium sporogenes ZP_02994961, pHY304 reverse	TCTAGAACTAGTGGATCCTCTATAGTTACTATGTTC
BBW3-32	Ruminococcus gnavus ZP_02040762, pHY304 forward	GTTTCCTCGAGCATCAGGAGGACAAAATC
BBW3-33	Ruminococcus gnavus ZP_02040762, pHY304 reverse	GTTTCTCTAGAAGACGATCTCCCAGTCTT
BBW3-34	Clostridium sporogenes ZP_02994961, pHY304 forward	GTTTCCTCGAGGGAATACCAGGAACTAAA
BBW3-35	Clostridium sporogenes ZP_02994961, pHY304 reverse	GTTTCTCTAGATCCATATGGTCCGTAGCT
BBW3-36	pTrc synthesis	CTCGAGTTGACAATTAATCATCCGGCTCGTATAATGTGT
BBW3-37	pTrc synthesis	TTGTTATCCGCTCACAATTCCACACATTATACGAGCCGGATG
BBW3-38	pTrc synthesis	GGAATTGTGAGCGGATAACAATTTCACACAGGAAACAGACCA
BBW3-39	pTrc synthesis	GTACCGAGCTCGAATTCCATGGTCTGTTTCCTGTGTGAAA
BBW3-40	pTrc synthesis	TGGAATTCGAGCTCGGTACGGATCCTCTAGATTTAAGAAGGAGA
BBW3-41	pTrc synthesis	ATGTATATCTCCTTCTTAAATCTAGAGGATCC
BBW3-42	t5Luc synthesis	GTCTTCACCTCGAGAAATCATAAAAAATTTATTTGCTTT
BBW3-43	t5Luc synthesis	CACATTATAATTGTTATCCGCTCACAAAGCAAATAAATTTTTTATGATTTCTCG
BBW3-44	t5Luc synthesis	GTGAGCGGATAACAATTATAATGTGTGAAATTGTGAGCGCTCGG
BBW3-45	t5Luc synthesis	ATGTATATCTCCTTCTTAAATCTAGAGGATCCGAGCGCTCACAATTTCA
BBW3-46	sequencing primer for pAH70 integration	AGGTTCTGCGCGGCGAAAA
BBW3-47	sequencing primer for pAH70 integration	TTCGTTATCGGCACTGGTCA
BBW3-48	Enterococcus faecalis 1kB upstream, pMAD forward	AATCTAGCTAATGTTACGTTACACATTAACTAGACAGATCT TCAATTGACTTTTACACA

BBW3-49	Enterococcus faecalis 1kB upstream, reverse (to assemble with 1kB downstream)	TTTTCCGTTTAAGATTCAATTAT TCACAACTTACACCCAAA
BBW3-50	Enterococcus faecalis 1kB downstream, forward (to assemble with 1kB upstream)	TTAGCCGTTTGGGTGTAAGTTGTGA ATAATTGAATCTTAAACG
BBW3-51	Enterococcus faecalis 1kB downstream, pMAD reverse	TCCATATGACGTCGACGCGTCTGCAGAAGCTTCTAGAATTCCAATTCCATTTTGCCATT
BBW3-52	pNS110 upstream sequencing primer	TCAAAACCTAAATTCACGTTGCC
BBW3-53	pNS110 downstream sequencing primer	TAATTTTATACACGTAAGTGATC
BBW3-54	Enterococcus faecalis, pAH70 forward	GTACCTCTAGACAGGAGACCATATGATGAATGCAAAATCTAAT
BBW3-55	Enterococcus faecalis, pAH70 reverse	ATTCGAGCTCGGTACCCGGGGATCCTTATTTTACGTCGTAAAT
BBW3-56	Enterococcus faecalis, pLT06 forward	CAGTATAAATTTAACGATCCCCGGGTACCGAGCTCGAATTCTCAATTGACTTTTACACA
BBW3-57	Enterococcus faecalis, pLT06 reverse	AATGGTTCGCTGGGTTTATCGACCTGCAGGTCGACTCTAGACAATTCCATTTTGCCATT
BBW3-58	sequencing primers	
BBW3-59	sequencing primers	
BBW3-60	sequencing primers	
BBW3-61	sequencing primers	
BBW3-62	chloramphenical (pLT06) into pMAD forward	AACGTTAAGGGATGCAGTTTATGCATCCCTTAACCTAAATCCAATCATCTACCCT
BBW3-63	chloramphenicol (pLT06) into pMAD reverse	AATTCATATAACCAAATTAAAGAGGGTTATAATGACTTTTAATATTATT
BBW3-64	pMAD for erm elimination forward	CTAAATCCAATCATCTACCCTGTTAAGGGATGCATAAACTGCATCCCTTAACTT
BBW3-65	pMAD for erm elimination reverse	ATGACTTTTAATATTATTTATAACCCTCTTTAATTTGGTTATATGAATT
BBW3-66	chloramphenical (pLT06) into pMAD forward	GGATGCAGTTTATGCATCCCTTAACTTACTCTAAATCCAATCATCTAC
BBW3-67	chloramphenicol (pLT06) into pMAD reverse	ATTCATATAACCAAATTAAAGAGGGTTATAATGACTTTTAATATTATT
BBW3-68	pMAD for erm elimination forward	AATAATATTAAAAGTCATATAACCCTCTTTAATTTGGTTATAT
BBW3-69	pMAD for erm elimination reverse	GTAGATGATTGGATTTAGAGTAAGTTAAGGGATGCATAAACTG
BBW3-70	646s IBS	AAAAAAGCTTATAATTATCCTTAGATTTCTATGCTGTGCGCCCAGATAGGGTG

BBW3-71	646s EBS1d	CAGATTGTACAAATGTGGTGATAACAGATAAGTCTATGCTAATAACTTACCTTTCTTTGT
BBW3-72	646s-EBS2	TGAACGCAAGTTTCTAATTTCGATTAAATCTCGATAGAGGAAAGTGTCT
BBW3-73	957s IBS	AAAAAAGCTTATAATTATCCTTATGCTACCTACGGGTGCGCCCAGATAGGGTG
BBW3-74	957s EBS1d	CAGATTGTACAAATGTGGTGATAACAGATAAGTCCTACGGACTAACTTACCTTTCTTTGT
BBW3-75	957s-EBS2	TGAACGCAAGTTTCTAATTTCGGTTTAGCATCGATAGAGGAAAGTGTCT
BBW3-76	1189s IBS	AAAAAAGCTTATAATTATCCTTACATGTCGAATTAGTGCGCCCAGATAGGGTG
BBW3-77	1189s EBS1d	CAGATTGTACAAATGTGGTGATAACAGATAAGTCGAATTAGATAACTTACCTTTCTTTGT
BBW3-78	1189s-EBS2	TGAACGCAAGTTTCTAATTTCGGTTACATGTCGATAGAGGAAAGTGTCT
BBW3-79	349s IBS	AAAAAAGCTTATAATTATCCTTAGGAACCGAAGCTGTGCGCCCAGATAGGGTG
BBW3-80	349s EBS1d	CAGATTGTACAAATGTGGTGATAACAGATAAGTCGAAGCTAATAACTTACCTTTCTTTGT
BBW3-81	349s-EBS2	TGAACGCAAGTTTCTAATTTCGATTGTTCCTCGATAGAGGAAAGTGTCT
BBW3-82 (BBW4-1)	742s IBS	AAAAAAGCTTATAATTATCCTTAGAGTGCAAAACGGTGCGCCCAGATAGGGTG
BBW3-83 (BBW4-2)	742s EBS1d	CAGATTGTACAAATGTGGTGATAACAGATAAGTCAAAACGGATAACTTACCTTTCTTTGT
BBW3-84 (BBW4-3)	742s-EBS2	TGAACGCAAGTTTCTAATTTCGATTCACTCTCGATAGAGGAAAGTGTCT
BBW3-82 (BBW4-1)	742s IBS	AAAAAAGCTTATAATTATCCTTAGAGTGCAAAACGGTGCGCCCAGATAGGGTG
BBW3-83 (BBW4-2)	742s EBS1d	CAGATTGTACAAATGTGGTGATAACAGATAAGTCAAAACGGATAACTTACCTTTCTTTGT
BBW3-84 (BBW4-3)	742s-EBS2	TGAACGCAAGTTTCTAATTTCGATTCACTCTCGATAGAGGAAAGTGTCT
BBW4-4	ZP_02995953 pET28 forward (03076)	CCTGGTGCCGCGCGGCAGCCATATGATGCTCTACTCTTCGAAA
BBW4-5	ZP_02995953 pET28 reverse (03076)	AGTGGTGGTGGTGGTGGTGCTCGAGTTCTAATGAGTAAATCCATA
BBW4-6	ZP_02993433 pET28 forward (00504)	CCTGGTGCCGCGCGGCAGCCATATGATGCTTGTTAATTCAACA
BBW4-7	ZP_02993433 pET28 reverse (00504)	AGTGGTGGTGGTGGTGGTGCTCGAGTTTTAACACATACCTGAAGA
BBW4-8	Ruminococcus gnavus ZP_02040762, pET28a Nde1	cctggtgccgcgcggcagccatatgatgagtcaagtaattaag

	forward	
BBW4-9	Clostridium sporogenes ZP_02994961, pET28a Nde1 forward	cctggtgccgcgcggcagccatatgatgaagttttggagaaaa
BBW4-10	Clostridium sporogenes ZP_02994961, pET24b Nde1 forward	actttaagaaggagatatacatatgatgaagttttggagaaaa
BBW4-11	Clostridium sporogenes ZP_02994961, pET28a Xho1 reverse	GTGGTGGTGGTGGTGGTGCTCGAGTttacattgcttttaagtg
BBW4-12	Clostridium sporogenes ZP_02994961, pET24b Xho1 reverse	agtggtggtggtggtggtgctcgagttacattgcttttaagtg

Publishing Agreement

It is the policy of the University to encourage the distribution of all theses and dissertations. Copies of all UCSF theses and dissertations will be routed to the library via the Graduate Division. The library will make all theses and dissertations accessible to the public and will preserve these to the best of their abilities, in perpetuity.

Please sign the following statement:

I hereby grant permission to the Graduate Division of the University of California, San Francisco to release copies of my thesis or dissertation to the Campus Library to provide access and preservation, in whole or in part, in perpetuity.

Author Signature

6/10/14

Date